

***Degradation of Monocrystalline Silicon Photovoltaic Cells/Modules  
under Heat and Temperature Effect***

***Géraud F. HOUNKPATIN*** <sup>(1,2)</sup>, ***Basile Bruno KOUNOUHEWA*** <sup>(1,2)</sup>,  
***Macaire AGBOMAHENA*** <sup>(3)</sup>, ***Vianou Irénée MADOGNI*** <sup>(1,2)\*</sup>

(1) Département de Physique (FAST) et Formation Doctorale Sciences des Matériaux (FDSM), Université d'Abomey-Calavi, Bénin

(2) Laboratoire de Physique du Rayonnement LPR, FAST-UAC, 01 BP 526 Cotonou, Bénin

(3) Laboratoire de Caractérisation Thermophysique des Matériaux et Appropriation Energétique (Labo CTMAE/EPAC/UAC), Abomey-Calavi, Bénin

**\*Corresponding Author:**

**E-mail Address:** madognimadogni@gmail.com

**Authors' contributions**

*GFH and BBK developed the general idea of the present research, carrying also out the literature review and manuscript preparation at early stages. The methodology and analytic procedures were carried out by VIM. Final review, including final manuscript correction has been done by BBK and AM. All authors were in charge of data generation/analysis and post-processing of the results.*

***Original Research Article***

**Abstract:**

PV-cell/module performance in general depends on solar irradiation (intensity, spectrum, especially ultraviolet (UV) radiation), temperature, moisture, mechanical stresses; and electrical operating conditions.

We investigated analytically the degradation of monocrystalline silicon PV cells/modules under heat and temperature effect.

Servant model has been exploited using the wind velocity under standard irradiation conditions ( $G=1000\text{W}/\text{m}^2$ ) in the 298-348K temperature range. The single exponential model has been used to extract the PV cell parameters from a single ( $J-V$ ) characteristic curve at various values of T.

The results obtained show that ( $J_{ph}$ ) increase exponentially from 7.67% to 65.87% with temperature. ( $R_s$ ) increase linearly by 7.6% and 9.18% while ( $V_{oc}$ ) decrease from 19.4 % to 17.6% and ( $R_{sh}$ ) decrease approximately by 12.6% and 4.8%. The obtained power output (P) losses had been 82.31 % and 31.56%, and the overall linear losses in efficiency ( $\eta$ ) had been approximately 27.84% and 5.02 %, while ( $J_s$ ) increase exponentially from 3.87% to 15.75%.

The increase in ( $J_{ph}$ ) with temperature can be attributed to the increased in light absorption owing to a decrease in the bandgap of silicon. The decrease in ( $\eta$ ) with temperature is mainly controlled by the decrease in ( $V_{oc}$ ) and fill factor (FF) with T.

**Keywords:** *Degradation; temperature and heat effect; Servant model; light absorption, decrease in the bandgap.*

## 1. Introduction

PV cells/modules know many degradation processes due to their exposure to temperature, atmospheric pressure, humidity, long time ultraviolet (UV) illumination, mechanical shock, precipitations, dust, wind and snow; which reduce the intrinsic lifetime of these cells very short. The limited lifetime is a result of several processes that are in play simultaneously [1, 2].

The yellowing, delamination, bubbles, breakage and cracks in the cells, defects in the anti-reflective coating, burnt cells, discoloration, and corrosion are the visible and dominant factors [1, 3-8]. Besides these direct defects, temperature can accelerate many degradation processes. The temperature plays then an important role in the photovoltaic cells/modules conversion process. The performance of these PV cells/modules decreases with increasing of the temperature, due to increased internal carrier recombination rates, caused by increased carrier concentrations [6]. In addition, combined effects (temperature and humidity; temperature and light; temperature, dust and humidity; light, humidity and dust) are factors of PV cells/modules degradation in almost all identified degradation modes [1-7].

The majority of studies on the crystalline Silicon (c-Si) technology report that the maximum power ( $P_{\max}$ ) degradation has been mainly attributed to short circuit current density ( $J_{SC}$ ) losses, followed by smaller decreases in the fill factor (FF). ( $J_{SC}$ ) degradation associated with the reduction of ( $P_{\max}$ ) has been most commonly caused by delamination and discoloration [8-13]. [12] Showed that the reduction in  $J_{SC}$  was due to discoloration or delamination at the cell/ethylene vinyl acetate (EVA) interface, front glass breakage and increased series resistance ( $R_S$ ), due to the degradation in electrode soldering. Interconnect degradation in crystalline silicon modules occurs when the joined cell-to-ribbon or ribbon-to-ribbon area changes in structure or in geometry. The characteristics directly attributable to interconnect degradation include increased series resistance ( $R_S$ ) in the electrical circuit, increased heating in the module, and localized hot spots causing burns at the solder-joints, at the polymer back sheet, and in the encapsulate [13,14].

The identification of the origin of degradation and failure modes and how they affect the photovoltaic cells/modules is necessary to improve the reliability of photovoltaic installations. However, despite the identification of PV modules degradation modes, it is still difficult to study them in real conditions. To overcome the obstacles of the long-term experiences, some analytical models have been elaborated in recent years, in order to study the degradation of the PV cells/modules under real conditions or not, since this depends on the aim at [1, 5, 15].

In this work, we used the Servant model under standard irradiation conditions to study analytically, the degradation of monocrystalline silicon PV cells under temperature and heat effect. The PV cell parameters have been extracted using the single exponential model in the 298-348 K temperature range.

Moreover, the environmental and climatic conditions in which the modules are exposed significantly influence the performance of these PV cells.

This paper is organized as follows. In Section 2, a visual inspection of PV modules degradation observed has been indexed. Subsequently, light-induced degradation, thermal degradation, electrical operating conditions have been established and presented. Next, the results are analyzed and discussed in section 3. Finally, in section 4, the conclusions and our perspectives are enumerated.

## 2. Materials and Methods

### 2.1. Visual degradation

Delamination is very frequent in hot and humid climates. It causes moisture penetration in the PV module and therefore induces various chemical and physical degradations such as metal corrosion of the module structure most frequently. Delamination is more severe if it occurs in the borders of the module because, a part from the power losses causes electrical risks to the module and the installation. Delamination is also related to a transmittance loss, as materials are not well optically coupled and a part of the light escapes [16-19] (**Fig.1**).

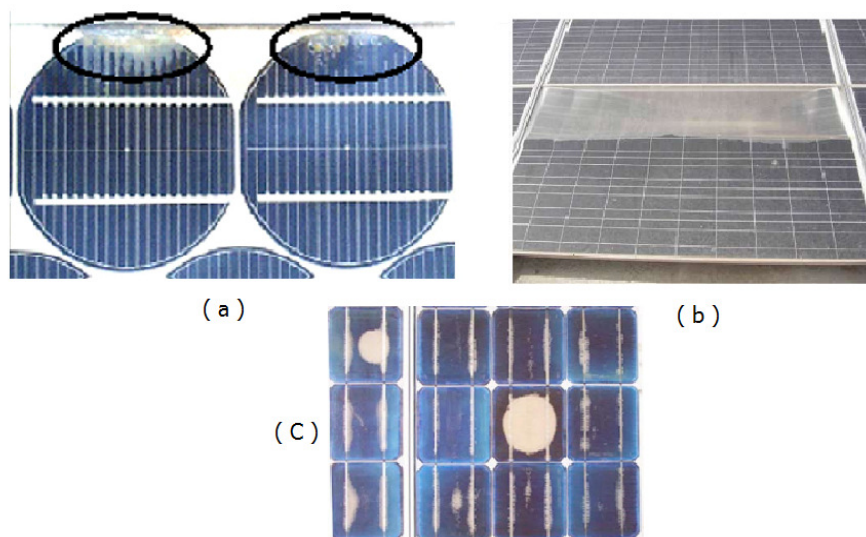


***Fig.1. (a) PV module délamination; (b)-(C) severe delamination (this figure presents an example of how an extreme delamination could destroy a PV module when the defect appeared after barely a year of functioning) [1, 16, 17]***

The corrosion attacks the metallic connections of PV cells causing a loss of performance by increasing leakage currents. Corrosion also degrades the adhesion between cells and metallic frame [3]. [20] Have been found out that corrosion appeared after 1000h of exposure of PV module under 85°C and 85% of relative humidity. Corrosion and discoloration are the predominant modes of photovoltaic modules degradation [3, 5] (**Fig.2**).

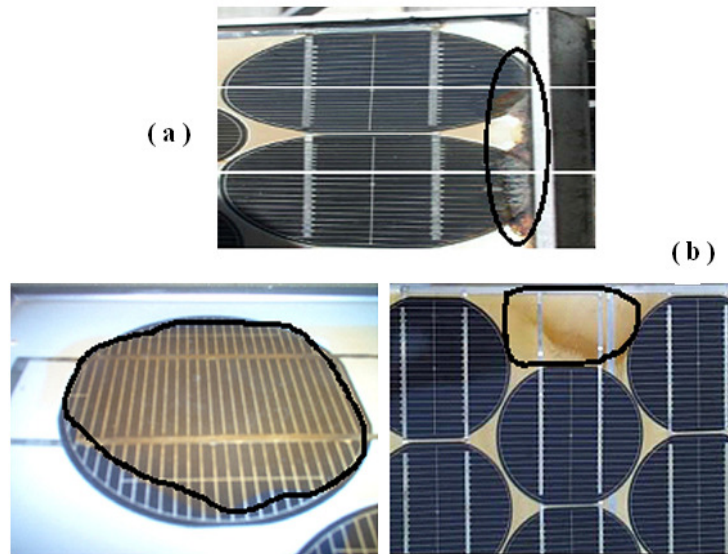


**Fig.2. (a) PV module affected by corrosion at the edge and the junction box [3]; (b) Solar cells discolored [1, 19]**

Module discoloration is a change in color of material which turns yellow and sometimes brown. It modifies transmittance of light reaching PV cells and therefore the power generated by the module is reduced. In addition, discoloration degrades the short-circuit current ( $I_{sc}$ ) of PV module. This degradation may vary from 6% to 8% below the nominal value for a partial discoloration of the PV module surface and from 10% to 13% for complete discoloration [1, 4, 21, 22, 23]. The Maximum power ( $P_{max}$ ) of the PV module is also degraded by module discoloration.

Glass breakage is one of an important degradation factor of PV cells/modules. Breakages and cracks are usually followed by other degradation types such as corrosion, delamination and discoloration [1, 13, 20] (**Fig.3**). Our investigations shown that, it is generally impossible to detect cracks on the already operational PV module to the naked eye. This detection can be done by using optical methods [24]. This method essentially consists of applying an intense wideband light (1000 suns) and detecting the path where the light passes through the cell or, on the contrary, is blocked due to the reflections that can cause a crack.

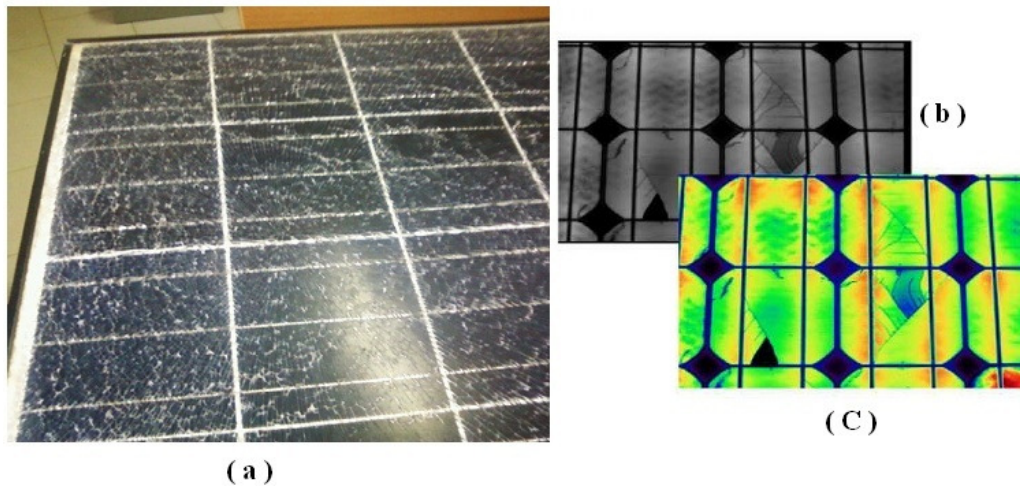


**Fig.3. (a) PV module with broken glass; (b) and (c) Cracks in cells. B & W image a simulated color image [1, 24].**

Cracks produce a loss in cell consistency and a possible carrier recombination path. They isolate parts of the cell avoiding the photocurrent generation. The effect of long-term exposure of the PV modules to a very high temperature, damages the cell or any other elements of the module [1]. This induces hot spots in some areas of the cell. Hot spots cause a variety of cell failures: shadowing, cells mismatch or failures in the interconnection between cells. This defective cell becomes a load for other cells, and a place of a relatively high thermal dissipation constituting thus a hot spot [1, 25]. Hot spots can cause damage to the cell or the encapsulant within a short time of operating (Fig. 4).

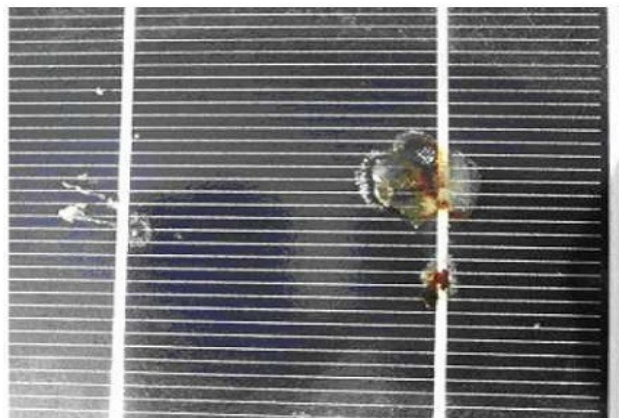


**Fig.4. Hot spot damages the PV cells/modules and reduces their performance [26]**

Thermal analysis has been used to detect a hot spot defect. This analysis could be performed in normal operation. In this case, the PV module could be operating in a solar plant. Another thermal test consists of the operation of the PV module at

extreme conditions (short-circuit conditions). In this case, the module should work alone, and the electrical connectors positive and negative of the module are short-circuited [1, 26].

Bubbles are generally due to chemical reactions that emit gases trapped in the PV cell/module (Fig.5).

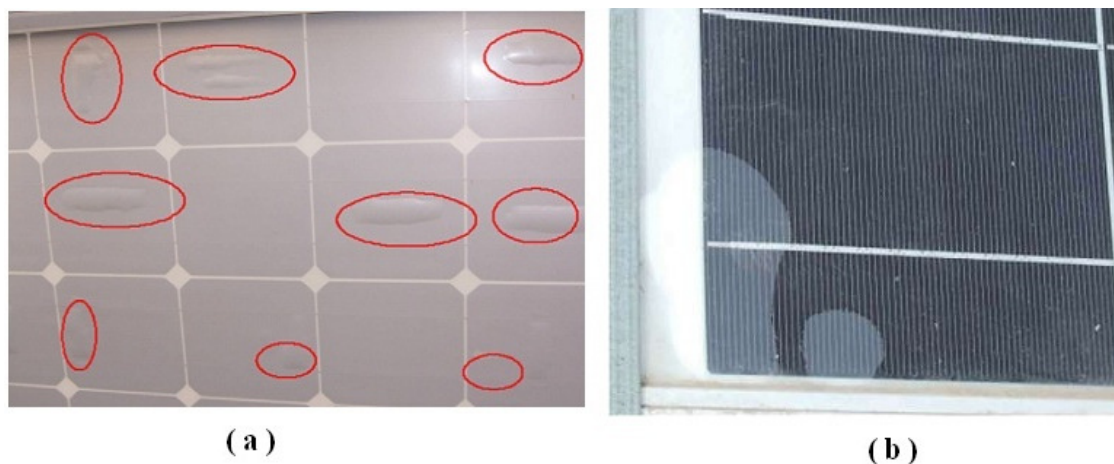


**Fig.5. (a) Bubbles on the back side of a PV module [1, 3]; (b) Bubbles on the front side of a PV module [24].**

Bubbles located on the module front side produce a reduction of the radiation reaching the module. Which cause a decoupling of the light and increase reflection [3]. This kind of defect is similar to delamination, but in this case, the lack of adherence of the EVA affects only a small area and is combined with the blowing of areas where this adherence has been lost. These defects appear in the center of the cell and may be due to poor adhesion of the cell caused by the high temperature. [1, 3]. When bubbles occur in the back side of the PV module, a bulk appears in the polymeric encapsulant or the back cover, forming a bubble. Bubbles make the heat dissipation of the cells more difficult, overheating them and subsequently reducing the lifetime of these cells. Bubbles have been detected using IR techniques [27], as they are not visible through visual inspection alone but rather cause a temperature change (Fig.5). In addition, the bubble forms an air chamber, and although the air temperature in the chamber appears lower than in the adjacent cells, the cell temperature is actually higher because the heat of the cell is less dissipated [26]. Moreover, the yellowing and browning cause a change in the transmittance of the light reaching the solar cells and thus a decrease in the power generated. The main cause of these defects in EVA and in ethylene copolymer films is UV radiation

and water exposure combined with temperatures above 50 °C that induce a change in the chemical structure of the polymer [21]. In some PV cells/modules, yellowing appears in some areas but not in adjacent areas with a different polymeric encapsulant of a different origin or characteristics. During the life of the PV module, the anti-reflective coating (ARC) receives radiation that could induce a change in the ARC coloring. The anti-reflective properties may suffer changes in this case. The light that reaches the cells may be lower than expected. Nonetheless, this colour change should not cause a decrease in the wavelength radiation that the cell uses, but rather only affect a part of the visible radiation. Anti-reflection coating is one of the light management techniques to reduce reflection loss of solar light. When the light passes through the interface between two media with different refractive index, partial light will be reflected back. In terms of solar cells, reflection will occur at device surface and each interfaces. Such reflected light will not be converted into electricity [28]. A follow-up of the affected modules should be done in order to detect whether this defect leads to another more severe defect [10]. Detachment of the frame, lines and blemishes in the cells are the other factors detected.

## **2.2. Light-Induced Degradation**

Possible degradation mechanisms under irradiance are presented in Fig.6. Light induced degradation is one of the main ageing mechanisms. More research is required to understand the mechanisms and kinetics of PV module discoloration as well as the induced power losses. Besides discoloration, bubbles are another concern for encapsulant photo-thermal degradation. In the process of photochemical degradation, gases of different types can be generated with a potential to cause delamination which can enhance water ingress and cause further problems such as decoupling of light transmission and reduction of heat dissipation. Another problematic reaction product generated during photochemical ageing is acid such as acetic acid and carbon dioxides.

The acidification may form electrolytes leading to metallization corrosion. It may also cause increased conductivity of the encapsulant which can result in increase leakage current. In addition, for the influences of irradiance on encapsulation materials, UV light has the most destructive effects. UV light is a primary initiator for many reactions such as the photodecomposition, photo thermal and photo bleaching. In contrast to discoloration, there is another UV-light induced effect called photo-bleaching as a result of photo-oxidation. With sufficient oxygen and at a high enough

temperature, the yellowed polyenes can be oxidized generating products that are more visibly clear. Photo-bleaching can lead to a color changing of EVA from yellow back to clear. Besides the photodegradation of the base material, additives within EVA will decompose under UV light, generating free radicals that accelerate base EVA photodecomposition. The generated products may be chromophores that can worsen EVA discoloration [29-32].

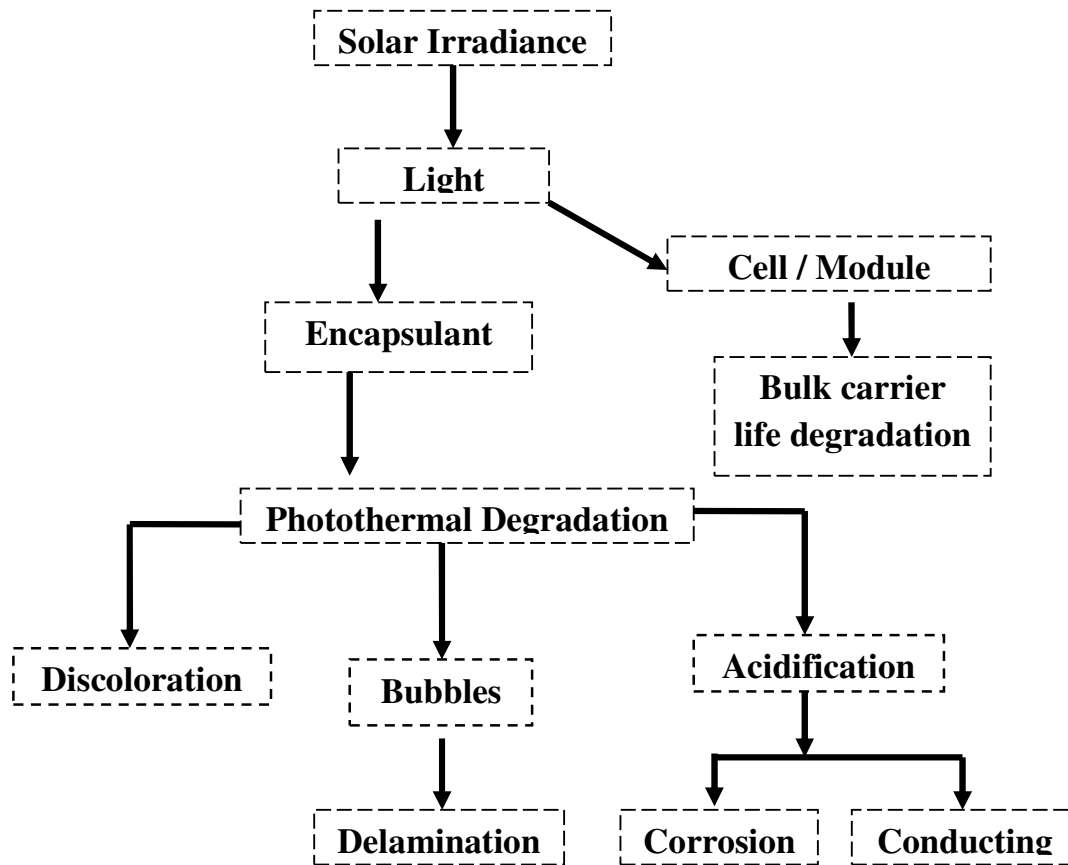


**Fig.6. Light-induced degradation**

### 2.3. Thermally-Induced Degradation

The temperature of cells/modules is usually higher than ambient temperature. Moreover, thermal effect acts as an accelerating factor for degradations caused by humidity or irradiance. Thermal cycles can reduce module reliability in a number of ways. For glass, residual strains may exist after lamination which can result breakage or delamination between glass/pottant under thermal strains. For encapsulant, different photo-thermal and thermal reactions can happen together with UV radiation from light. The principal reactions of EVA are what called Norrish I and Norrish II. In Norrish I, the vinyl acetate group can take off from the main chain to

form acetaldehyde together with some gases which have potential to further lead to bubbles in the module. In Norrish II, C=C bonds (polyenes) are formed which have been widely considered as the chromophores group for EVA discoloration. Besides that, acetic acid is produced to catalyze discoloration and corrosion reaction.

The polyenes produced in Norrish II can further be oxidized to form  $\alpha$ - $\beta$  unsaturated carbonyl, another product leading to discoloration [6, 33, 34]. Besides chemical reactions, polymer may also undergo morphology changes under high temperature. Cells can also suffer from thermal fatigue with reported cracking and solder joint degradation. With regards to interfaces, the thermal heterogeneity of different materials can induce cracks, bubbles and delamination under daily thermal cycles. Besides these direct defects, temperature can accelerate many degradation processes. The water diffusion through polymers has been reported to be accelerated by temperature in the Arrhenius form [35]. Other procedures like metallization corrosion, leakage current, diffusion of dopants, impurities, occur more rapidly at higher temperature.

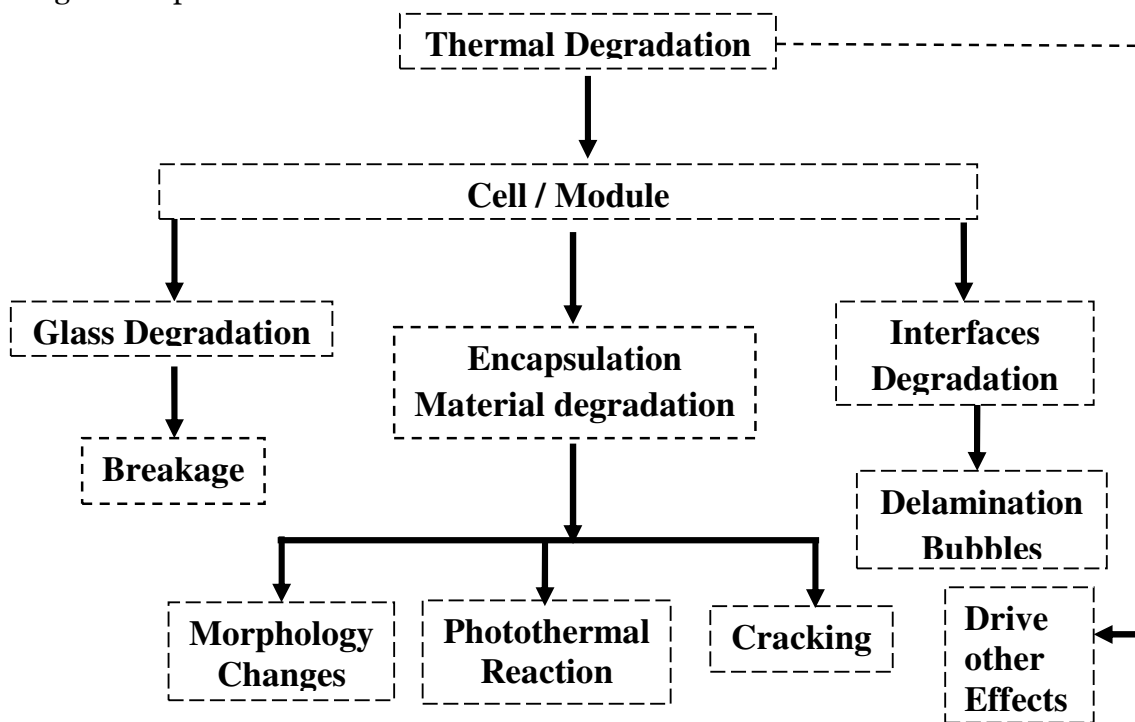


**Fig.7. Thermal-induced degradation**

## 2.4. Electrical operating conditions

Most of the electrical parameters of PV modules depend on the temperature and the solar irradiation. Once all these parameters are determined within reference conditions, their new values can be determined in any real operating conditions [36-42], using the following models (1)-(19) indexed.

### 2.4.1. Photocurrent density ( $J_{ph}$ )

In most of the studies, the photocurrent density ( $J_{ph}$ ) is approximated by the short circuit current density [38, 43, 44]. This assumption is generally accepted for the modeling of PV module or cell because in real devices the series resistance is low while the parallel resistance is high. This parameter is often considered as a good starting point in several defined iterative algorithms [39].

$$J_{ph}(G, T) = J_{ph_{ref}} \left[ 1 + \alpha_{J_{SC}} (T_m - T_{ref}) \right] \frac{G}{G_{ref}} \quad (1)$$

Where  $T_{ref}$  : solar cell temperature in reference condition,  $G_{ref}$ : solar irradiation in reference condition,  $G$ : solar irradiation,  $T_m$ : module temperature,  $\alpha_{J_{SC}}$ : Temperature coefficient of the short-circuit current density (available in the module data sheet),  $J_{ph_{ref}}$ : short-circuit current density in the reference conditions.

### 2.4.2. Saturation current density ( $J_S$ )

The rates of the saturation current density change with the cell temperature according to equations (2, 3) and (4, 5) for one-diode [38] and two-diode model [39, 45] respectively. Authors report that the equations are suitable for all technology of silicon solar cells [38, 39, 45].

$$J_S = J_{S_{ref}} \times \left( \frac{T_m}{T_{ref}} \right)^3 \times \exp \left( \frac{1}{K} \left( \frac{E_{g_{ref}}}{T_{ref}} - \frac{E_g(T_m)}{T_m} \right) \right) \quad (2)$$

$$\frac{E_g(T)}{E_{g_{ref}}} = 1 - 0.0002677 (T_m - T_{ref}) \quad (3)$$

$$J_{S_i} = J_{S_{ref}} \times \left( \frac{T_m}{T_{ref}} \right)^{\frac{3}{ni}} \times \exp \left( \left( \frac{E_g(T)}{ni.K} \right) \left( \frac{1}{T_{ref}} - \frac{1}{T_m} \right) \right) \quad (4)$$

with  $i = 1, 2$

$$E_g(T) = 1.17 - 0.000673 \times \frac{T_m^2}{T_m + 636} \quad (5)$$

with  $J_{S_{ref}}$ ,  $J_S$  the saturation current density in reference and real conditions respectively,  $K$ : Boltzmann constant ( $J.K^{-1}$ ),  $E_g$ (eV): Gap of the semi-conductor material in the real conditions is linked for one-diode model to the gap in reference conditions by expression (5) which has been widely used for silicon solar [38]: The value of  $E_{g_{ref}}$  for the silicon solar cells at STC conditions is equal to 1.121eV [38].

### 2.4.3. Series ( $R_S$ ) and shunt ( $R_{Sh}$ ) resistance

Several methods have been used to calculate series ( $R_S$ ) and shunt ( $R_{Sh}$ ) resistance values at non STC conditions from their reference values (data known at given conditions) [38, 46]. In general, the methods require material (semi-conductor) characteristic coefficients. These latter vary from one module to another and must be experimentally determined. To simplify the calculation, some authors assume that  $R_S$  is independent of incident irradiation and temperature for both one-diode models [36, 47, 48] and two-diode model [39, 49]. It has been reported that shunt resistance is inversely proportional to the solar irradiance [36, 37, 50]. [39, 51] have shown that this earlier assumption is true only at very low light intensities while  $R_{Sh}$  is considered independent of temperature and can be set constant for  $G > 100 \text{ W/m}^2$ . Unfortunately, these two assumptions lead to bad results with [42] modeling especially for two-diode models. It seems that the right way to determine  $R_S$  and  $R_{Sh}$  should take into account the thermal parameters of the material. Nevertheless, the following methods [36-38] give good results for the two types of model.

$$\frac{R_S}{R_{S_{ref}}} = \frac{T_m}{T_{ref}} \left( 1 - \beta \times \ln \frac{G}{G_{ref}} \right) \quad (6)$$

Where  $\beta$ , is a coefficient which value is approximately 0.217 and  $R_{S_{ref}}$ : Series resistance in the reference conditions

$$R_{Sh_{ref}} = R_{Sh} \times \frac{G}{G_{ref}} \quad (7)$$

In addition, Series resistance is known to affect Fill factor (FF) adversely. [52] Have observed that  $R_S$  decreases more rapidly with  $T$  in the low temperature region (100–250 K) in poly silicon cells as compared to that in single-crystal cells. [53] Have found that  $R_S$  increases with temperature. [54] Have found that ideality factor  $n$  of a solar cell decreases with  $T$ . Earlier studies [55, 56] have ignored the effect of temperature dependence of  $R_{sh}$  on  $dV_{OC}/dT$  and that of temperature dependence of  $R_S$  on (FF) and are applicable only for higher efficiency cells which have very low  $R_S$  and very

large  $R_{Sh}$  values. We have noticed that in case of cells having screen-printed contacts solar cells  $R_S$  may be high and  $R_{Sh}$  may be low and both may vary with T significantly.

#### 2.4.4. Open-circuit voltage( $V_{OC}$ )

The main temperature dependence in solar cells arises from variation of three main parameters, which are usually used to characterize the solar cell outputs, these are:  $J_{SC}$ , the short-circuit current density, which usually has a negative sign, the open-circuit voltage  $V_{OC}$  which in principal is characterized by  $J_S$ , the diode saturation current, and n, the diode ideality factor, and the fill factor FF, which in turn is a function of  $V_{OC}$ .  $V_{OC}$  is given as follows [57]:

$$V_{OC} = \frac{n k T_m}{q} \ln \left[ 1 - \frac{G_{Sh} V_{OC}}{J_S} + \frac{J_{ph}}{J_S} \right] \quad (8)$$

Where  $J_S$  : is a function of material properties and it is also sensitive to temperature. According to Eq. (9),  $T_m$ : module temperature. We expect a linear dependence of  $V_{OC}$  on temperature, if  $J_{ph} \gg G_{Sh} V_{OC}$  and  $J_{ph} \gg J_S$ , then, we have:

$$V_{OC} = \frac{E_g}{q} - \frac{n k T_m}{q} \ln \left( \frac{J_S}{J_{ph}} \right) \quad (9)$$

$E_g$ : Bandgap energy of the absorber material.

#### 2.4.5. PV module efficiency models

The performance of a solar cell is influenced by temperature as its performance parameters: open-circuit voltage ( $V_{OC}$ ), short-circuit current density ( $J_{SC}$ ), fill factor (FF) and efficiency ( $\eta$ ) are temperature dependent. It has been shown earlier that  $V_{OC}$  decreases at a rate of 2.3 mV/K whereas  $J_{SC}$  increases slightly with temperature ( $T_m$ ). (FF) also decreases and all these lead to an overall decrease in the cell efficiency [58].

It turns out that both the open circuit voltage and the fill factor decrease substantially with temperature (as the thermally excited electrons begin to dominate the electrical properties of the semi-conductor), while the short-circuit current increases, but only slightly [58, 59]. All these effects lead to a linear relation in the form:

$$\eta = \eta_{T_{ref}} \left[ 1 - \beta_{ref} (T_m - T_{ref}) + \gamma \log_{10} G_T \right] \quad (10)$$

$\eta_{T_{ref}}$ : Module electrical efficiency at the reference temperature,  $T_m$ : PV module temperature,  $T_{ref}$ : Reference temperature at solar radiation flux of 1000W/m<sup>2</sup>,

$\beta_{ref} = \frac{1}{T_O + T_{ref}}$ : Temperature coefficient (depends not only on the PV material but

on  $T_{ref}$ ),  $\gamma$  : Solar radiation coefficient and  $T_0$ : the high temperature at which the PV module's electrical efficiency drops to zero [58, 60, 61].

A reduced expression of the model has been proposed by [62], neglecting the solar radiation coefficient (for a weak solar radiation):

$$\eta = \eta_{T_{ref}} [1 - \beta_{ref} (T_m - T_{ref})] \quad (11)$$

In these analytical models, the cell/module temperature which is not readily available has been replaced by the nominal operating cell temperature ( $T_{NOCT}$ ) and we have [63]:

$$\eta = \eta_{ref} \left\{ 1 - \beta_{ref} \left[ T_a - T_{ref} + (T_{NOCT} - T_a) \frac{G_T}{G_{NOCT}} \right] \right\} \quad (12)$$

In which

$$T_a = T_m - \left( \frac{G_T}{G_{NOCT}} \right) \left( \frac{U_{L,NOCT}}{U_L} \right) (T_{NOCT} - T_{a,NOCT}) \left[ 1 - \left( \frac{\eta_c}{\tau \alpha} \right) \right] \quad (13)$$

An analytical model of the monthly average efficiency has been proposed by [64], in order to estimate the monthly electrical energy output of a PV array.

$$\bar{\eta} = \eta_{T_{ref}} \left[ -1 - \beta_{ref} (\bar{T}_a - T_{ref}) - \frac{\beta_{ref} (\bar{\tau} \alpha) \bar{H}_T \bar{V}}{n U_L} \right] \quad (14)$$

Where,  $n$  : Number of hours per day,  $U_L$  : overall thermal loss coefficient,  $\bar{H}_T$  : the monthly average daily insolation on the plane of the array,  $\bar{V}$  : a dimensionless function of such quantities as the sunset angle.

#### 2.4.6. PV module power output models

The prediction of PV module performance in terms of electrical power output in the field, that is, the deviation from the standard test conditions reported by the manufacturer of the module, is analytically modeled in a manner analogous to the module efficiency. Recently, [65] proposed a correlation for PV module power, similar in form to Eq. (11).

$$P = G_T \tau_{pv} \eta_{ref} A [1 - 0.0045 (T_m - 25)] \quad (15)$$

$\tau_{pv}$ ; Transmittance of the PV cell outside layers

A nonlinear multivariable regression model has been proposed by [66], resulting from an analysis which addresses the fact that the cells within a module are not identical

$$P_{mp} = d_1 G_T + d_2 T_m + d_3 [\ln(G_T)]^m + d_4 T_m [\ln(G_T)]^m \quad (16)$$

In which ‘m’ are model parameters.

Another unusual nonlinear correlation has been proposed by [67], giving a correction coefficient for the output power as defined by Eq. (17) of a water cooled PV system:

$$P_m = V_m I_m = (FF) \times V_{OC} \times I_{SC} \quad (17)$$

$$P = V_C I_C \left[ 1 - \frac{G_T - 500}{2 \times 10^4} + \frac{C_{TC}}{4 \times 10^4} \times (50 - T_m)^2 \right] \quad (18)$$

$I_C$  and  $V_C$  are the output voltage and current respectively

The wind speed is taken into account in several correlations for the efficiency [58, 66, 68-71].

$$P = G_T (b_1 + b_2 G_T + b_3 T_a + b_4 V_f) \quad (19)$$

In which  $V_f$  : represents the free-stream local wind speed, measured at a height of 10m above ground,  $b_j, j = 1, 4$ : regression coefficients, are determined using solar radiation flux values above  $500 \text{ W/m}^2$ .

Besides, [68] review the methods proposed in the literature to determine the operating temperatures of the modules. These models can be classified into implicit and explicit.

The implicit model is based on the knowledge of the thermal properties of the module and their heat transfer mechanisms. An energy balance in the module is thus considered, from which it is possible to determine its instantaneous operation temperature. The practical application of this type of models is very complicated, as they require the module to be in a steady state. This is difficult to meet under real operating conditions, and the temperature of the module greatly depends on the meteorological parameters, which are continuously changing, and the thermal processes that occur in the different materials that make up the module [72].

The explicit methods calculate the operating temperature of the module using known parameters. Thus, the simplest expression is the one that uses the nominal operating cell temperature, which is widely used and supplied by the module manufacturers. This temperature is defined under specific meteorological conditions that are difficult to meet under real conditions [58, 73].

## 2.5. Cell temperature models

The cell temperature is a function of the ambient temperature  $T_a$  and the solar irradiation  $G$ . It is generally approximated with the following expression [57, 58, 74].

$$T_m = T_{amb} + \frac{G}{800} (T_{NOCT} - 293.15^\circ K) \quad (20)$$

$T_{NOCT}$  : Nominal temperature of the PV cells at a solar irradiation of 800 W/m<sup>2</sup>, an ambient temperature of 20°C and a wind speed of 1ms<sup>-1</sup>.

In practice, the sizing in many PV systems and the simulation of their operating is carried out using hourly and, sometimes, even daily values [75]. [76] Puts forward another model to obtain the temperature of the module based on a simplified model of the heat exchange between the PV module and the atmosphere. All these models work with instantaneous value of all the parameters and predict the value of the temperature of the module for a specific instant.

### 2.5.1. Servant model

This model is based on the heat exchange between the PV module and the atmosphere. He allows obtaining the temperature of the module according to meteorological parameters [76].

$$T_m = T_{amb} + d \times G \times (1 + e \times T_{amb})(1 - fW) \quad (21)$$

Where W: the wind speed, d, e and f : Parameters that are calculated empirically.

### 2.5.2. Ross model

Based on the thermal properties of the module when steady state, [77] proposes a model where the difference between the temperature of the module and the ambient temperature is directly proportional to the incident irradiance:

$$T_m = T_{amb} + K \times G \quad (22)$$

K: the Ross coefficient depends, among other factors, on the technology of the module, its shape and size, encapsulation, assembly and environmental conditions.

### 2.5.3. King model

In order to offset the influence that wind speed has on the temperature of the module, a ratio between the module temperature, the incident irradiance and the wind speed has been proposed [58].

$$T_m = T_{amb} + G \times e^{(m+n.W)} \quad (23)$$

G: Incident solar irradiance on the surface of the module,  $m$ : Dimensionless empirical coefficient that describes the impact of the irradiance on the temperature of the module, establishing the upper limit of the temperature of the module at low wind speeds and high irradiances,  $n$ : Empirical coefficient that describes the cooling

of the module because of the wind; in other words, the speed at which the temperature of the module drops as the wind speed increases.

#### 2.5.4. Mattei model

This model is based on the energy balance that takes place in the module. The temperature of a module according to this model is given by the following expression [72]:

$$T_m = \frac{U_{PV}T_{amb} + G [(C_{\alpha}\tau) - \eta_r - \gamma \eta_r T_r]}{U_{PV} - \gamma \eta_r G} \quad (24)$$

where  $U_{PV} = p + qW$ : Heat exchange coefficient of the module depending on the wind speed,  $C_{\alpha}$ : Cell absorption coefficient,  $\tau$ : Glass transmittance,  $\eta_r$ : The efficiency of the module at the benchmark temperature  $T_r = 25^{\circ}\text{C}$  and at an irradiance of  $1000\text{W}/\text{m}^2$  and  $\gamma$ : The absolute value of the variation coefficient of the power with the temperature of module in %C.

Two new models have been proposed that, based on the standard NOCT model, means that the influence of the wind speed on the operating temperature of the module can be introduced.

##### ❖ NOCT-1p model

The NOCT model assumes that wind speed is always 1m/s. When a module is exposed to real sunlight, the wind speed has many different values. Therefore, this model takes into account the impact of the wind speed on the temperature of the module.

$$T_m = T_{amb} + \frac{G}{800 \text{ W}/\text{m}^2} (\text{NOCT} - 20^{\circ}\text{C}) + a (W + W_1) \quad (25)$$

where  $W_1$ : The benchmark wind speed that appears in the definition of the NOCT temperature ( $W_1=1\text{m}/\text{s}$ ),  $W$ : Wind speed in m/s and  $a$ : an empirical parameter, expressed in  $^{\circ}\text{C} \cdot \text{s} \cdot \text{m}^{-1}$ . These values are determined in the experimental fitting of the data.

##### ❖ NOCT-2p model

This model takes into account the relationship between the temperature increase and the incident irradiance.

$$T_m = T_{amb} + b \left[ \frac{G}{800 \text{ W}/\text{m}^2} (\text{NOCT} - 20^{\circ}\text{C}) \right] + C (W + W_1) \quad (26)$$

Where  $b$ : Dimensionless parameter,  $C$ : has the same dimensions and meaning as in the previous model.

### 2.5.5. Hourly models

Using the previously described instantaneous models, new models have been built where the baseline data are the hourly values of the different meteorological variables that appear in each of the models. These new hourly models are proposed both for the previously existing instantaneous models and for the ones proposed by [74]. The hourly value is the average value of all the instantaneous measurements recorded in that hour, except for the hourly irradiation that is the integral of the irradiance values logged in that time interval.

#### 2.5.5.1. Hourly nominal operating cell temperature model

$$T_{m-h} = T_{amb-h} + \frac{H}{800 \text{ Wh/m}^2} (NOCT - 20^\circ\text{C}) \quad (27)$$

where,  $T_{m-h}$ : The average temperature of the module in one hour ( $^\circ\text{C}$ ),  $T_{amb-h}$ : The hourly mean of the ambient temperature ( $^\circ\text{C}$ ),  $H$ : The hourly irradiation received by the module ( $\text{Wh/m}^2$ ).

#### 2.5.5.2. Hourly Servant model

$$T_{m-h} = T_{amb-h} + d_h H (1 + e_h T_{amb-h}) (1 - f_h W_h) \quad (28)$$

$W_h$ : Hourly average of the wind speed,  $d_h$ ,  $e_h$  and  $f_h$  the parameters to be determined that will now,  $d_h$  have different units to the constant of the instantaneous model.

#### 2.5.5.3. Hourly Ross model

$$T_{m-h} = T_{amb-h} + k_h H \quad (29)$$

$k_h$ : The empirical coefficient expressed in ( $^\circ\text{C.m}^2/\text{Wh}$ ).

#### 2.5.5.4. Hourly King model

[78] Proposed a modification to the equation (23), for instantaneous values, in order to eliminate the dimensional inconsistency.

$$T_{m-h} = T_{amb-h} + \frac{T_O}{H_O} H (e^{m_h + n_h W_h}) \quad (30)$$

$T_O$  and  $H_O$ : are the ambient temperature and irradiation in standard measurement conditions,  $m_h$  and  $n_h$  are now the parameters to be determined.

If the equation of King's instantaneous model, Eq (23), had been applied, the hourly expression obtained would be as follows:

$$T_{m-h} = T_{amb-h} + \frac{T_O}{H_O} H (e^{m_{h-h} + n_{h-h} W_{h-h}}) \quad (31)$$

Where  $m_{h-h}$  and  $n_{h-h}$  represent the values of those parameters in King's original model. Matching the Eqs (30) and (31), the following relationships have been obtained:

$$\begin{cases} n_{h-h} = n_h \\ m_{h-h} = m_h - \ln \frac{H_0}{T_0} = m_h - \ln 40 \end{cases} \quad (32)$$

### 2.5.5.5. Hourly Mattei model

$$T_m = \frac{(P_h + q_h W_h) T_{amb-h} + H [(C_{\alpha\tau})_h - \eta_r - \gamma \eta_r T_r]}{P_h + q_h W_h - \gamma \eta_r H} \quad (33)$$

Where  $(C_{\alpha\tau})_h$ : the new empirical coefficients to be determine, that continues to be dimensionless,  $P_h$ : expressed in  $(Wh.m^{-2} \circ C^{-1})$  and  $q_h$  expressed in  $(Wh.s.m^{-3} \circ C^{-1})$ .

### 2.5.5.6. Hourly NOCT-1p model.

$$T_{m-h} = T_{amb-h} + \frac{H}{800 Wh/m^2} (NOCT - 20^\circ C) + a_h (W_k - W_1) \quad (34)$$

Where  $W_1 = 1m/s$  and  $a_h$ : the parameter to be determined in  $(^\circ C. s. m^{-1})$ . When  $W_h = 1$ , this model coincides with the NOCT model.

### 2.5.5.7. Hourly NOCT-2p model.

$$T_{m-h} = T_{amb-h} + b_h \left[ \frac{H}{800 Wm^{-2}} (NOCT - 20^\circ C) \right] + C_h (W_h + W_1) \quad (35)$$

Where  $b_h$  continues to be a dimensionless parameter and  $C_h$  is expressed in  $(^\circ C. s.m^{-1})$ .

## 3. Results and Discussions

### 3.1. Sharp NTS5E3E module characteristics

Sharp NTS5E3E photovoltaic module considered is constituted of 72 monocrystalline silicon cells (125.5mm×125.5mm), connected in series with a maximum power 185Watts.

#### ❖ *Under the standard test conditions:*

- Sunshine: 1000 W/m<sup>2</sup>, atmospheric mass (AM): 1.5, module temperature (T): 25°C;
- Open-circuit voltage (V<sub>OC</sub>): 44.9 V, the peak voltage (V<sub>pm</sub>): 36.21V;
- Short-circuit density (J<sub>SC</sub>): 5.60 A, the peak current-density (J<sub>pm</sub>): 5.11A;
- The peak power (P<sub>maxc</sub>): 185.0 W, yield of the encapsulated cell ( $\eta_c$ ): 17.1 %, module yield ( $\eta_m$ ): 14.2 %.

#### ❖ *Relative coefficients to the temperature:*

- Power( $\alpha_{p_{max}}$ ): - 0,485 A / °C ;

- Short-circuit density ( $\alpha_{J_{SC}}$ ) : + 0,053 A /°C ;
- Open-circuit voltage ( $\alpha_{V_{OC}}$ ) : -156 Mv /°C

❖ **Analytical characteristics:**

The structure of Sharp NTS5E3E photovoltaic module is modeled by the equivalent electrical circuit (Fig. 7) with a single diode [2].

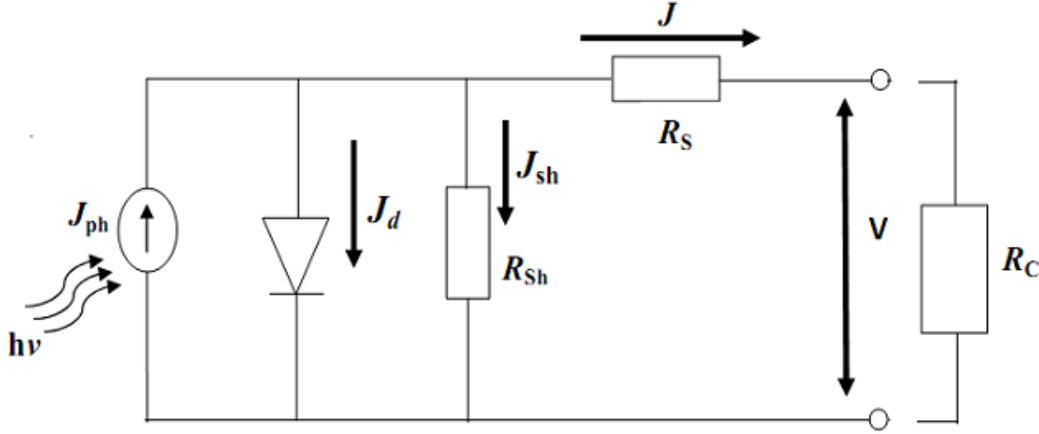


**Fig.8. Equivalent electrical circuit of Sharp NTS5E3E photovoltaic module under an incident illumination**

According to the nodes and meshes laws, we have:

$$J + J_{ph} = J_d + J_{sh} \quad \text{and} \quad V = JR_s + J_{sh} \times R_{sh} \quad (36)$$

Using the expression for the current-voltage characteristic of PV, we find the expression for  $J$  as:

$$J = J_{ph} - J_s \left[ \exp\left(\frac{q(V + R_s J)}{n k_B T}\right) - 1 \right] - \frac{(V + R_s J)}{R_{sh}} \quad (37)$$

Therefore, the transcendental analytic equation for the optimal current  $J_{opt}$  of the ideal PV module is described by [79]:

$$J_{opt} = \frac{J_{ph} + J_s}{1 + \frac{1}{\ln\left(\frac{J_{ph} - J}{J_s} + 1\right)}} \quad (38)$$

With, 
$$V_{opt} = \frac{k T_m}{q} \ln\left(\frac{J_{ph} - J}{J_s} + 1\right) \quad (39)$$

Where  $J_{ph} (A/cm^2)$  : the photoinduced current-density determined by the spectral composition, intensity, and concentration of incident solar radiation and also by the efficiency of assembling photogenerated p-n junction charge carriers,  $J_s (A/cm^2)$  : the reverse dark photoinduced saturation current-density determined by potential and electro-physical

parameters of p-n junction,  $T_m$ (°K): PV module temperature,  $k$ : the Boltzmann constant; and  $q$ (C) is the electron charge.

When the PV module is illuminated by solar light  $J_{Ph} \gg J_S$ ,  $J_{Ph} - J \gg J_S$ , the logarithm in the denominator of  $J_{opt}$  is a higher value and does not vary much with variations in  $J$ . Then, the transcendental equation is solved by stepwise approximations. For  $J = 0$ , we have:

$$J_{opt} = \frac{J_{Ph}}{1 + \frac{1}{\ln\left(\frac{J_{Ph}}{J_S}\right)}} \quad (40)$$

and the optimal voltage becomes:

$$V_{opt} = \frac{k T_m}{q} \left[ \ln\left(\frac{J_{Ph}}{J_S}\right) - \ln \ln\left(\frac{J_{Ph}}{J_S}\right) \right] \quad (41)$$

The analytical peak power is finally expressed as:

$$P_{opt} = J_{opt} \times V_{opt} = \frac{J_{Ph}}{1 + \frac{1}{\ln\left(\frac{J_{Ph}}{J_S}\right)}} \times \frac{k T_m}{q} \left[ \ln\left(\frac{J_{Ph}}{J_S}\right) - \ln \ln\left(\frac{J_{Ph}}{J_S}\right) \right] \quad (42)$$

### 3.2. Working principle

The module considered is an inorganic photovoltaic device represented by its band diagram (**Fig.9**). His photon flux conversion into electrical energy is based on three mechanisms [79].

- the incident photons absorption by the active material constituting the device;
- electron-hole pairs creation in the semiconductor material;
- Collect of the charge-carriers photogenerated in the device.

An incident photon is absorbed in the photoactive semiconductor if the photon energy is higher than the bandgap ( $E_g$ ) of the semiconductor. This excites an electron from the valence band to the conduction band leaving a positively charged hole in the valence band. The electron and hole are then extracted at the contacts to the outer circuit.

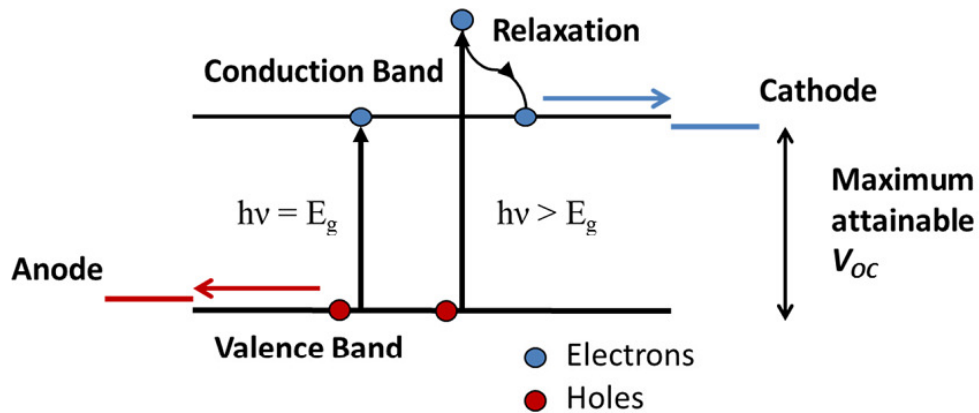


**Figure. 9. Working principle of the solar cell**

A small  $E_g$  is desirable in order to absorb as many photons as possible. However for photons with  $h\nu > E_g$  the extra energy is lost to thermodynamical relaxation [80 - 83]. In general, assuming solar light generation, the lower the bandgap the higher the  $J_{SC}$  and the lower the  $V_{OC}$ , hence there is some optimal bandgap that maximizes the product of the  $J_{SC}$  and the  $V_{OC}$ . Using the principle of detailed balance, the maximum achievable efficiency for a single junction solar cell at room temperature to be 44% and the optimal bandgap to be 1.1eV [83]. Taking further losses into account they furthermore showed that the highest attainable  $\eta$  for a single junction cell is 31% under practical circumstances.

### **3.3. Causes and effects of degradation (Visual characteristics)**

We indexed the modes of degradation and mechanisms along with cause and effect in association with the encapsulant in photovoltaic cells/modules [84]

#### **3.3. 1. Corrosion**

##### **❖ Causes**

- Moisture ingress through or laminate edges
- Presence of higher ambient temperature along with humidity
- High system voltage due to sunlight presence
- Higher ionic conductivity of encapsulant due to moisture
- Higher moisture absorption of encapsulant
- Metallization sensitivity to moisture
- Interconnect sensitivity to moisture

##### **❖ Effects**

- Hotspot induced backskin burns
- Hotspot induced broken glass
- Power drop beyond warranty limit due to severe series resistance

##### **❖ Mechanism**

- Chemical corrosion (metallic and semiconducting components during nighttime), electrochemical corrosion (metallic components during daytime), or photoelectrochemical corrosion (semiconducting components during daytime) between cells or between cell and frame.

### **3.3. 2. Encapsulant delamination**

#### **❖ Causes**

- Sensitivity of adhesive bonds to ultraviolet (UV) light at higher temperatures or to humidity in the field
- Poor adhesive bonds at the interfaces during processing (glass/encapsulant; cell/encapsulant; backsheet/encapsulant)
- Contamination from the material (excess in glass or acetic acid from encapsulant)

#### **❖ Effects**

- Moisture ingress
- Enhanced encapsulant conductivity and interface conductivity (enhanced chemical/ electrochemical/photoelectrochemical corrosion)
- Major transmission loss
- Power drop beyond warranty limit due to optical decoupling and moisture ingress induced corrosion

#### **❖ Mechanism**

- Photothermal reaction (interface bonds breakage due to UV and temperature)
- Chemical reaction (interface bond breakage because of humidity or contaminants)

### **3.3. 3. Degradation Mode Slow corrosion**

#### **❖ Causes**

- Moisture ingress through backsheet or laminate edges
- Presence of higher ambient temperature along with humidity
- High system voltage due to sunlight presence
- Higher ionic conductivity of encapsulant due to moisture
- Higher moisture absorption of encapsulant
- Metallization(alloy) sensitivity to moisture
- Interconnect (alloy) sensitivity to moisture

❖ **Effects**

- Increase in series resistance and decrease in power but within warranty limit

❖ **Mechanism**

- Chemical corrosion (metallic and semiconducting components during nighttime), electrochemical corrosion (metallic components during daytime) between cells or between cell and frame

**3.3.4. Gradual electrochemical corrosion or cation migration to the semiconductor surface/junction**

❖ **Causes**

- Moisture ingress through backsheet or laminate edges
- Higher ionic conductivity of encapsulant due to moisture
- Higher moisture absorption of encapsulant
- Metallization (alloy) sensitivity to moisture
- Interconnect (alloy) sensitivity to moisture

❖ **Effects**

- Series resistance increase and : or shunt resistance decrease depending on bias polarity and climatic conditions
- Potential induced degradation leading to power loss but within warranty limit

❖ **Mechanism**

- Electrochemical corrosion (metallic components during daytime or photoelectrochemical corrosion (semiconducting components during daytime are more sensitive to electrochemical reactions under light) between cell and frame.

**3.3. 5. Gradual backsheet warping /detaching/cracking/crumbling**

❖ **Cause**

- Poor adhesion between encapsulant and backsheet
- Moisture ingress through backsheet and /or laminate edges
- Polymer disintegration over time

❖ **Effects**

- Slow power degradation (due to corrosion of cell and circuit components but within warranty limit.

❖ **Mechanism**

- Chemical reaction weakening interface bonds (due to higher ambient temperature and / or humidity)

**3.3. 6. Gradual encapsulant discoloration**

❖ **Causes**

- UV exposure at higher operating temperatures
- Reduced breathability
- Higher UV concentration
- Inappropriate additives in EVA

❖ **Effects**

- Transmission loss Reduced current/power but may not be affecting fill factor or warranty limit Cosmetic/visual change

❖ **Mechanism**

- Photothermal reaction (in the presence of UV and higher module temperature)

**3.4. Electrical parameters degradation correlated with visual degradation**

**Tableau1:** Electrical parameters influencing on PV cells performance

Parameters	dependency	Influential factor
Cell density photocurrent	Depend on	Irradiance and wavelength
$V_{oc}$	Logarithmically dependent on	illumination
$J_{sc}$	Dependent on	illumination
Fill factor	Increases by	I1/Is increase
Fill factor	Increases by	Series resistance decrease
Fill factor	Increases by	Shunt resistance increase
$V_{oc}$	Decreases by	Temperature rise
$J_{sc}$	Nearly constant by	Temperature rise
Fill factor	Decreases by	Temperature rise

In addition, we established a qualitative correlation between the electrical parameters affected and the different modes of degradation listed. However, the effect of discoloration causes loss of transmittance of the encapsulant EVA, reducing the photocurrent density ( $J_{ph}$ ) of the cell/module thus culminating in decreased absorption of sunlight by the photovoltaic cell/module and power loss [1, 85, 86].

The position of EVA discoloration on solar cell results degradation of ( $J_{SC}$ ) because it reduces the current flowing through the solar cell. It has been found that the discoloration does not affect the fill factor (FF) and ( $V_{oc}$ ) more. However there are significant effect on the ( $J_{SC}$ ) degradation and hence the power output (P) degradation [86, 87]. The corrosion of the edge, the junction box, bus-bars and interconnects cause the degradation of the PV modules peak power ( $P_{max}$ ). The rate of power degradation is more in case of high corrosion of string interconnect ribbon. Then, with increase of percentage defects, the rate of power degradation increases. More recently, [87] shown that the power degradation range in Bus-bar is 0-2.1% per year, in cell interconnection ribbon is 0-2.1% per year and in string interconnection ribbon is 1-2.3% per year. The range of power degradation varies from 2.08% to 3.48% per year and the average degradation has been 2.60% per year in the case of EVA discoloration for only seven PV modules analyzed.

Delamination in the back-sheet of the PV module reduces the thermal conductivity locally and hence increases the cells/modules temperature.

We revealed that the delamination depends on the detachment of the two layers, EVA-glass and EVA-back-sheet. The delamination occurring in back-sheet, the range of power degradation varies from 3.17 to 3.63%/year [86-88]. Hot spot occurs in PV modules due to thermal expansion/contraction of interconnection, shadowing, faulty cell and low resistance cell resulting decrease in ( $J_{SC}$ ) and power. As the daily average power increases with decrease in number of hot spots, the range of the power degradation has been 0.29%/year for no hot spot and 2.16%/year for four hot spot and total power degradation after 22 years outdoor exposure has been 6.38% for no hot spot and 47.52% for four hot spot [87]. As a result, while a number of hot spot increases the area covered by the hot spot also increases.

In a general way, environmental and climatic conditions in which the modules are exposed significantly influence degradation. PV-module performance in general depends on solar irradiation (intensity, spectrum, especially ultraviolet (UV) radiation), temperature, moisture, mechanical stresses; and electrical operating conditions [89]. Other regional climate factors must be considered: snow, hail, wind, salt, sand, dust, and pollutants/gases, some of which are potentially corrosive.

Temperature is extremely significant to the degradation process, especially hot spots, encapsulant bleaching, delamination failure on interconnections, etc. Temperature is responsible for most of the chemical reactions of the degradation of modules. Elevated temperatures can drastically change the mechanical, electrical, and optical properties of polymeric materials. Rapid changes in temperature over a short period of time cause thermo-mechanical stress and induce defects that can alter critical properties of polymer [87-89].

The long-term damage to the EVA during its useful life often involves interaction between heating at temperatures above 353K, absorption of moisture, oxygen, and most importantly, ultraviolet (UV) radiation from the solar spectrum. UV radiation has been identified as a critical factor in the degradation of photovoltaic modules by many research groups, and chemical changes in its structure have been identified leading to changes in transmission (discoloration). Thus, photodegradation caused by UV radiation is a major degradation of the material exposed to direct sunlight, and degradation is certainly climate zone dependent since the solar spectrum can change significantly from one geographical area to another [84-89].

### 3. 5. Numerical Simulation (Electrical operating conditions)

Servant model is based on the heat exchange between the PV module and the atmosphere. It allows obtaining the temperature of the module according to meteorological parameters Eq. (21) [76].

$$T_m = T_{amb} + d \times G(1 + e \times T_{amb})(1 - f \times W)$$

where W: Wind speed and d, e, f: Empirical parameters;  $T_{amb}$ : ambient temperature.

#### 3.3.1. Photocurrent Density ( $J_{ph}$ )

$$J_{ph}(G, T) = J_{ph_{ref}} \left[ 1 + \alpha_{J_{SC}} (T_m - T_{ref}) \right] \frac{G}{G_{ref}}$$

$$J_{ph}(T_{amb}) = \frac{G J_{ph_{ref}}}{G_{ref}} \left[ 1 + \alpha_{J_{SC}} (T_{amb} + d \times G(1 + e_0 T_{amb})(1 - f_0 W) - T_{ref}) \right]$$

$$= \frac{\alpha_{J_{SC}} \cdot G \cdot J_{ph_{ref}}}{G_{ref}} \left[ \frac{1}{\alpha_{J_{SC}}} - T_{ref} + T_{amb} + d \times G(1 + e_0 \times T_{amb})(1 - f_0 W) \right]$$

**Variables declaration:**

$$J_{phref} = 5.11A/m^2 ; G_{ref} = 1W/m^2 ; G = 1000 W/m^2$$

$$\alpha_{jsc} = u = 7.5 \times 10^{-2} ; T_{ref} = 298 K ; d = 2.1 \times 10^{-2} \text{ } ^\circ C.m^2/w ;$$

$$e_0 = 1.6.10^{-20} C^{-1} ; f_o = 7.5 \times 10^{-2} ; W = 1.1 \times 10^{-3} m/S$$

$$t = \frac{u \times G \times J_{phref}}{G_{ref}} ; p = \frac{1}{u} ; t_1 = p - T_{ref} ; S = d \times G \times (1 - f_o \times W)$$

$$J_{ph}(T_{amb}) = t \times [t_1 + T_{amb} + S \times (1 + e_0 \times T_{amb})] \quad (43)$$

### 3.3.2. Series resistance ( $R_S$ )

$$\frac{R_S}{R_{Sref}} = \frac{T_m}{T_{ref}} \left( 1 - \beta \times \ln \frac{G}{G_{ref}} \right)$$

$$R_S(T_{amb}) = R_{Sref} \times \frac{T_m}{T_{ref}} \left( 1 - \beta \times \ln \frac{G}{G_{ref}} \right)$$

$$T_m = T_{amb} + d \times G(1 + e_0 \times T_{amb})(1 - f_o W)$$

$$R_S(T_{amb}) = \frac{R_{Sref}}{T_{ref}} (T_{amb} + d \times G(1 + e_0 \times T_{amb})(1 - f_o W)) \left( 1 - \beta \times \ln \frac{G}{G_{ref}} \right)$$

**Variables declaration:**

$$R_{Sref} = 5.11 \Omega ; T_{ref} = 298 K ; u = \beta = 4.5.10^{-1} ; G = 1000 W/m^2$$

$$d = 2.1 * 10^{-2} \text{ } ^\circ C.m^2/w ; G_{ref} = 1w/m^2 ; e_0 = 1.6.10^{-20} C^{-1} ; f_o = 7.5 \times 10^{-2} ;$$

$$W = 1.1 \times 10^{-3} m/S ; t_1 = \frac{R_{Sref}}{T_{ref}} ; ; V = \frac{G}{G_{ref}} ; t_2 = (1 - u \times \ln(V))$$

$$t = t_1 \times t_2 \text{ and } S = d \times G \times (1 - f_o W)$$

$$R_S(T_{amb}) = t \times (T_{amb} + S \times (1 + e_0 \times T_{amb})) \quad (44)$$

### 3.3.3. PV module efficiency ( $\eta$ )

$$\eta = \eta_{T_{ref}} [1 - \beta_{ref}(T_m - T_{ref}) + \gamma \times \log G_T]$$

$$T_m = T_{amb} + d \times G(1 + e_0 \times T_{amb})(1 - f_o W)$$

$$\eta = \eta_{T_{ref}} [1 + \gamma \times \log (G) + \beta_{ref} \times T_{ref} - \beta_{ref} \times (T_{amb} + d \times G(1 + e_0 \times T_{amb})(1 - f_o W))]$$

**Variables declaration :**

$$T_{ref} = 298 \text{ } ^\circ K ; d = 2.110^{-2} C.m^2/w ; e_0 = 1.5.10^{-20} C^{-1} ; \beta_{ref} = V = 4.5 \times 10^{-3} ; n_{ref} = 1.5 \times 10^{-1} \% ; \gamma = u = 5.3 \times 10^{-4} ; G = 1000 W/m^2$$

$$f_o = 7.5 \times 10^{-2}; W = 1.1 \times 10^{-3} \text{ m/S}$$

$$t = 1 + u \times \log(G); t_1 = V \times T_{ref}; t_2 = t + t_1; S = d \times G \times (1 - f_o W).$$

$$\eta(T_{amb}) = \eta_{T_{ref}} \times [t_2 - V \times (T_{amb} + S \times (1 + e_0 \times T_{amb}))] \quad (45)$$

### 3.3.4. PV module power output (P)

$$P(T_{amb}) = G \times \tau_{pV} \times \eta_{ref} \times A \times [1 - V \times (T_m - T_{ref})]$$

$$T_m = T_{amb} + d \times G \times (1 + e_0 \times T_{amb})(1 - f_o W)$$

$$p(T_{amb}) = G_T \tau_{pV} \eta_{ref} A [1 + V \times T_{ref} - V \times (T_{amb} + d \times G \times (1 + e_0 \times T_{amb})(1 - f_o W))]$$

**Variables declaration:**

$$G = 1000 \text{ W/m}^2; n_{ref} = 1.5 \cdot 10^{-1} \%; \tau_{pV} = u = 3.8 \cdot 10^{-1}; A = 4;$$

$$V = 4.5 \times 10^{-3}; d = 2.1 \times 10^{-2} \text{ C m}^2/\text{W}; T_{ref} = 298 \text{ K};$$

$$e_0 = 1.5 \times 10^{-2} \text{ }^\circ\text{C}^{-1}; f_o = 7.5 \times 10^{-2}; W = 1.1 \times 10^{-3} \text{ m/S}$$

$$p_1 = A \times G \times u \times \eta_{ref}; t = 1 + V \times T_{ref} \text{ and } S = d \times G \times (1 - f_o W).$$

$$p(T_{amb}) = p_1 \times [t - V \times (T_{amb} + S \times (1 + e_0 \times T_{amb}))] \quad (46)$$

### 3.3.5. Shunt resistance ( $R_{Sh}$ )

$$R_{Sh} = R_{Sho} - m_o \times T_m$$

$$T_m = T_{amb} + d \cdot G(1 + e_0 T_{amb})(1 - f_o W)$$

$$R_{Sh}(T_{amb}) = R_{Sho} - m_o [T_{amb} + d \cdot G(1 + e_0 T_{amb})(1 - f_o W)]$$

$$R_{Sh}(T_{amb}) = m_o \times \left[ \frac{R_{Sho}}{m_o} - T_{amb} - d \times G \times (1 + e_0 \times T_{amb})(1 - f_o W) \right]$$

**Variables declaration:**

$$m_o = 6.8936 \text{ } \Omega\text{C m}^2/\text{K}; R_{Sho} = 3858.86 \text{ } \Omega\text{C m}^2/\text{K}; d = 2.1 \times 10^{-2} \text{ C} \cdot \text{m}^2/\text{W};$$

$$G = 1000 \text{ W/m}^2; e_0 = 1.5 \times 10^{-2} \text{ }^\circ\text{C}^{-1}; f_o = 7.5 \times 10^{-2};$$

$$W = 1.1 \times 10^{-3} \text{ m/S}; u = \frac{R_{Sho}}{m_o} \text{ and } S = d \times G \times (1 - f_o W)$$

$$R_{Sh}(T_{amb}) = m_o \times [u - T_{amb} - S \times (1 + e_0 \times T_{amb})] \quad (47)$$

### 3.3.6. Open-circuit voltage ( $V_{OC}$ )

$$V_{OC}(T_{amb}) = \frac{E_g}{q} - \frac{nkT_m}{q} \times \ln\left(\frac{J_S}{J_{ph}}\right)$$

$$T_m = T_{amb} + d \times G(1 + e_0 \times T_{amb})(1 - f_o W)$$

$$V_{OC}(T_{amb}) = \frac{E_g}{q} - \frac{nk}{q} (T_{amb} + d \times G \times (1 + e_0 \times T_{amb})(1 - f_o W)) \times \log\left(\frac{J_S}{J_{ph}}\right)$$

**Variables declaration:**

$$E_g = 1.884 \times 10^{-19} \text{Joule}; \quad n = 1.25; \quad q = 1.6 \cdot 10^{-19} \text{C}; \quad J_{ph} = 5.11 \text{ A/m}^2;$$

$$J_S = 0.9 \text{ A/m}^2; \quad G = 1000 \text{ W/m}^2; \quad k = 1.38 \times 10^{-23};$$

$$d = 2.1 \times 10^{-2} \text{ C} \cdot \text{m}^2/\text{W}; \quad e_0 = 1.5 \times 10^{-2} \text{ }^\circ\text{C}^{-1}; \quad f_o = 7.5 \times 10^{-2};$$

$$W = 1.1 \times 10^{-3} \text{ m/S}; \quad t = \frac{n \times k}{q}; \quad u = \frac{J_S}{J_{ph}}; \quad p = \log(u); \quad t_1 = \frac{E_g}{q};$$

$$S = d \times G \times (1 - f_o \times W); \quad t_3 = p \times t \quad \text{and} \quad t_4 = \frac{t_1}{t_3}$$

$$V_{OC}(T_{amb}) = t_3 \times (t_4 - T_{amb} - S \times (1 + e_0 \times T_{amb})) \quad (48)$$

### 3.3.7. Saturation current density ( $J_S$ )

$$J_S = J_{S_{ref}} \times \left(\frac{T_m}{T_{ref}}\right)^{\frac{3}{ni}} \times \exp\left(\left(\frac{E_g(T)}{n \times K}\right)\left(\frac{1}{T_{ref}} - \frac{1}{T_m}\right)\right)$$

$$T_m = T_{amb} + d \times G \times (1 + e_0 \times T_{amb})(1 - f_o W)$$

$$J_S = J_{S_{ref}} \times \left(\frac{T_{amb} + d \times G \times (1 + e_0 \times T_{amb})(1 - f_o W)}{T_{ref}}\right)^{\frac{3}{n}} \times \exp\left(\left(\frac{E_g(T)}{n \times K}\right)\left(\frac{1}{T_{ref}} - \frac{1}{T_{amb} + d \times G \times (1 + e_0 \times T_{amb})(1 - f_o W)}\right)\right)$$

**Variables declaration:**

$$J_{S_{ref}} = 1.2 \cdot 10^{-3} \text{ A/m}^2; \quad T_{ref} = 298 \text{ }^\circ\text{K}; \quad d = 2.1 \times 10^{-2} \text{ }^\circ\text{C} \times \text{m}^2/\text{W};$$

$$G = 1000 \text{ W/m}^2; \quad e_0 = 1.5 \times 10^{-2} \text{ }^\circ\text{C}^{-1}; \quad f_o = 7.5 \times 10^{-2};$$

$$W = 1.1 \times 10^{-3} \text{ m/S}; \quad n = 1.25; \quad E_g(T) = 1.884 \times 10^{-19} \text{ Joule};$$

$$k = u = 1.38 \times 10^{-23}; \quad u = \frac{3}{n}; \quad t = \frac{E_g(T)}{n \times k}; \quad t_1 = \frac{1}{T_{ref}}; \quad s = d \times G;$$

$$z = 1 - f_o \times W; \quad t_2 = s \times z \quad \text{and} \quad t_3 = t_1 \times t_2$$

$$J_S(T_{amb}) = J_{S_{ref}} \times (t_1 \times T_{amb} + t_3 \times (1 + e_0 \times T_{amb}))^u \times \exp\left(t \times \left(t_1 - \frac{1}{T_{amb} + t_2 \times (1 + e_0 \times T_{amb})}\right)\right) \quad (49)$$

### 3.4. Interpretation of the results simulated

It is necessary to study the performance of solar cells under variable solar irradiance intensities and temperatures in order to be able to provide the accurate prediction of the energy production of PV systems. In this study, the dependence of performance parameters ( $J_{Ph}$ ), ( $R_S$ ), ( $V_{OC}$ ), ( $R_{Sh}$ ), ( $P$ ), ( $\eta$ ) and ( $J_S$ ) under the illumination intensity of  $1000 \text{ W/m}^2$  at different temperatures is shown in **Fig.10** to **Fig.16**. The parameters ( $V_{OC}$ ) (**Fig.10**), ( $R_{Sh}$ ) (**Fig.11**), and ( $\eta$ ) (**Fig.12**), decrease linearly with T while ( $R_S$ ) (**Fig.13**) increase linearly with ambient temperature.

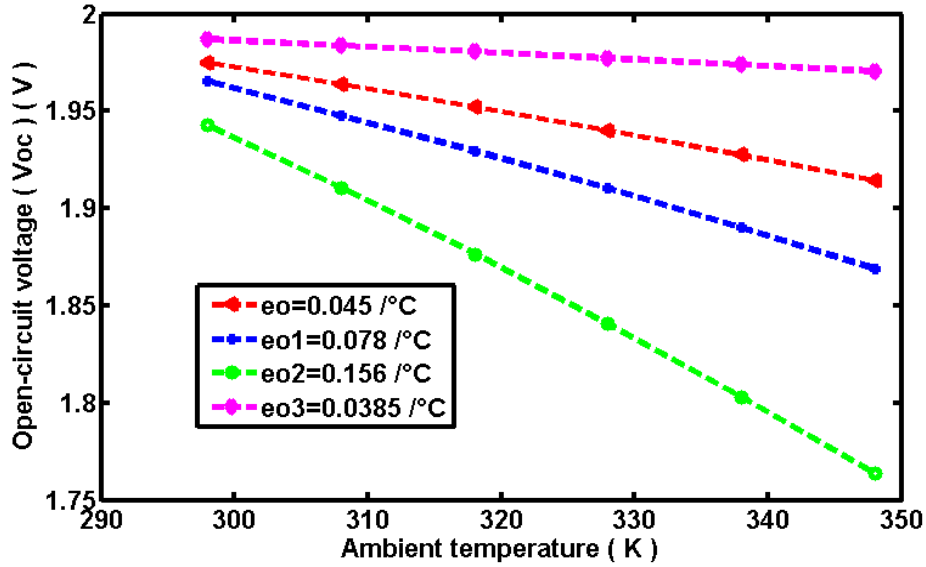


**Fig.10. Normalized plot of open-circuit voltage ( $V_{OC}$ ) with temperature in the range 295-348 K. This curve is analytically obtained from (Eq.48) as a function of the ambient temperature**

In addition, ( $J_{Ph}$ ) (**Fig.14**) and ( $J_S$ ) (**Fig.15**) increase exponentially with temperature, while the obtained power output ( $P$ ) (**Fig.16**) decrease exponentially.

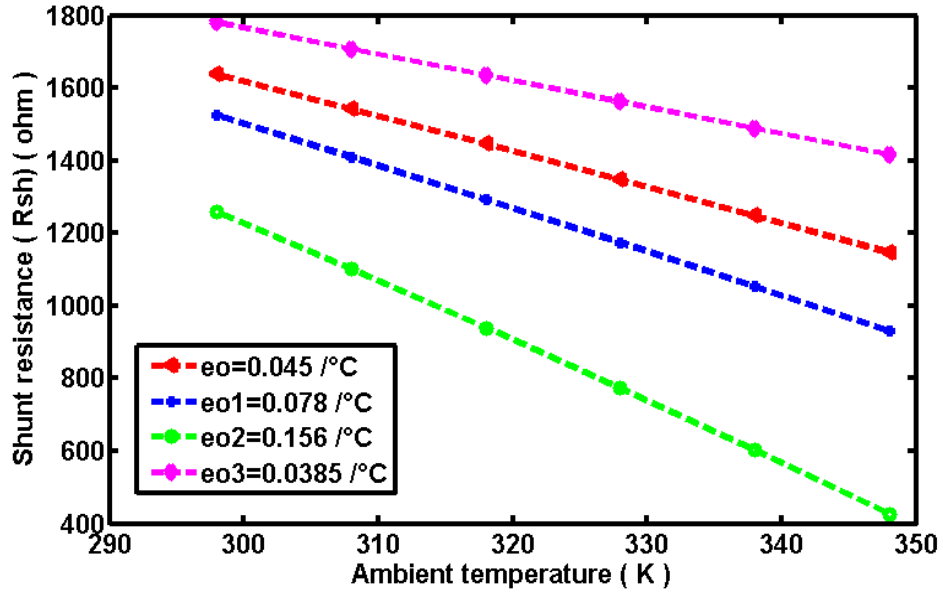


Fig.11. Normalized plot of shunt resistance ( $R_{sh}$ ) with temperature in the range 295-348 K. This curve is analytically obtained from (Eq.47) as a function of the ambient temperature

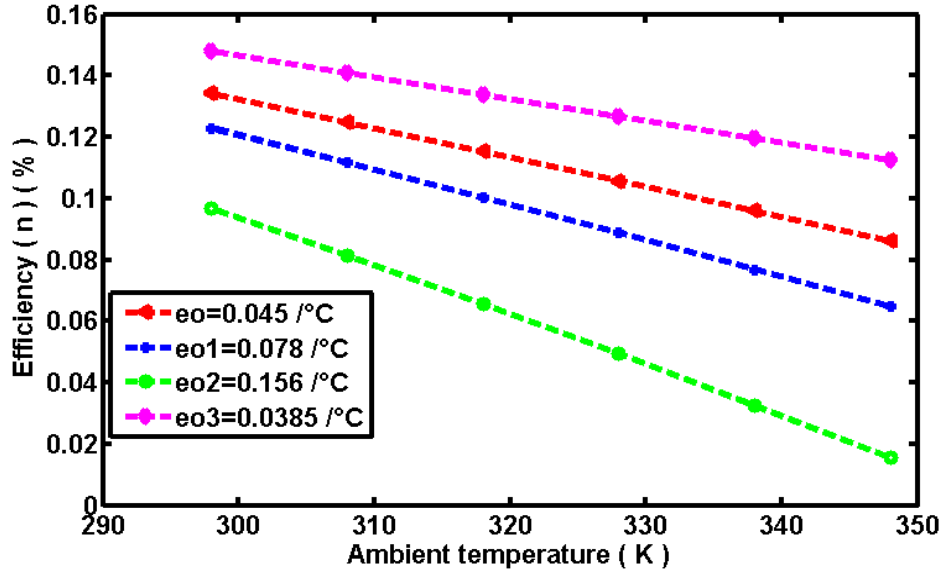


Fig.12. Normalized plot of Efficiency ( $\eta$ ) with temperature in the range 295-348 K. This curve is analytically obtained from (Eq.45) as a function of the ambient temperature

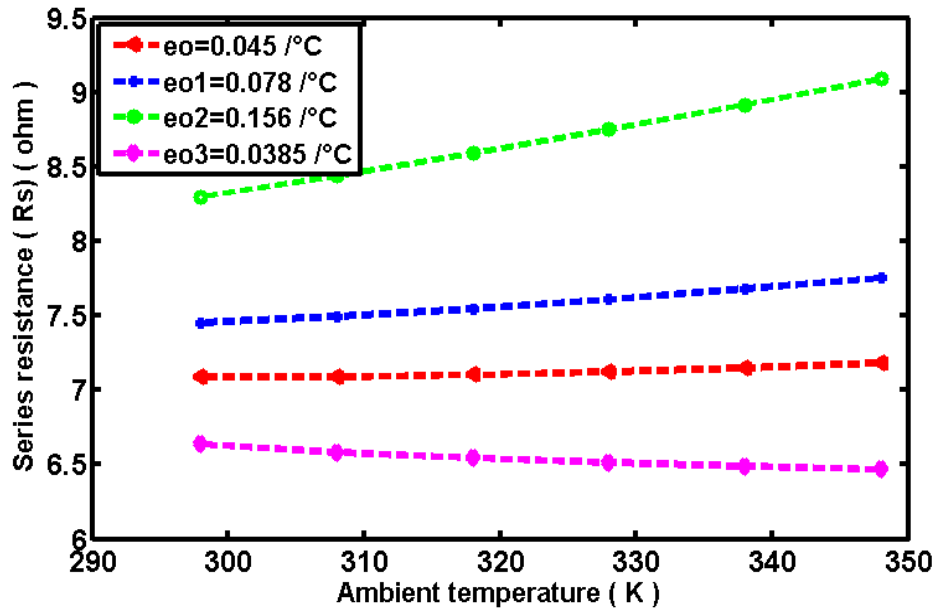


Fig.13. Normalized plot of series resistance ( $R_S$ ) with temperature in the range 295-348 K. This curve is analytically obtained from (Eq.44) as a function of the ambient temperature

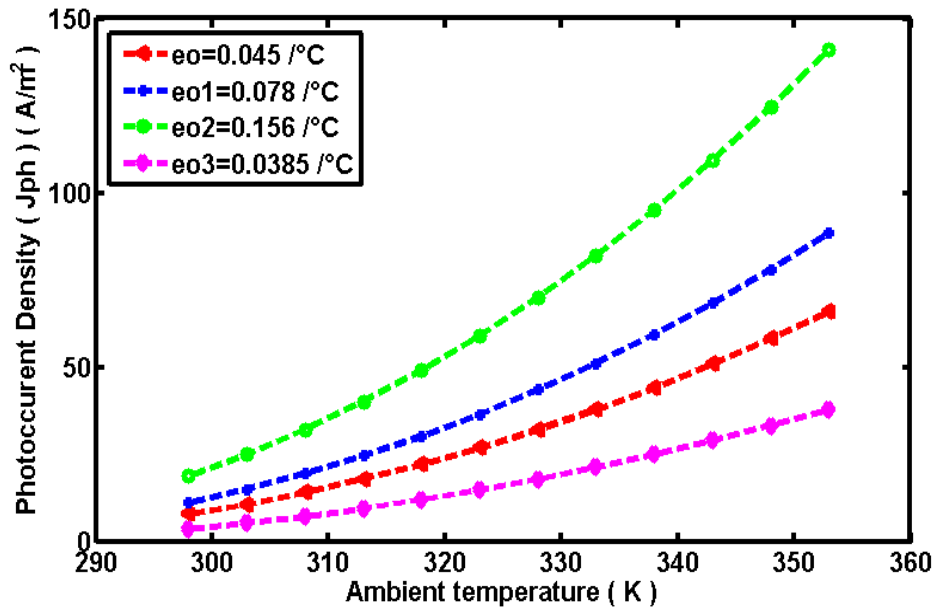


Fig.14. Normalized plot of photocurrent density ( $J_{ph}$ ) with temperature in the range 295-353 K. This curve is analytically obtained from (Eq.43) as a function of the ambient temperature

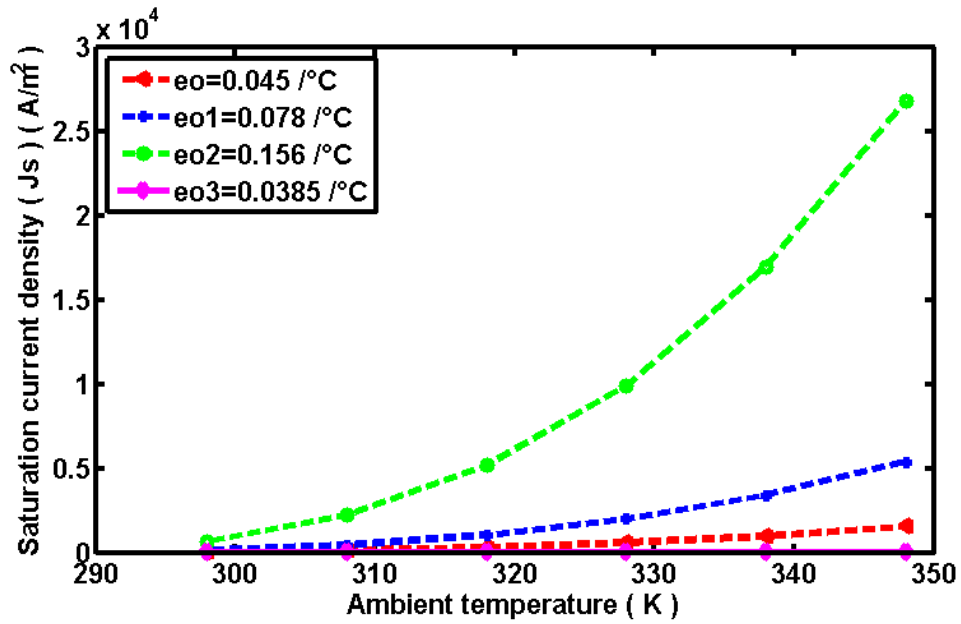


Fig.15. Normalized plot of Saturation current density ( $J_s$ ) with temperature in the range 295-348 K. This curve is analytically obtained from (Eq.49) as a function of the ambient temperature

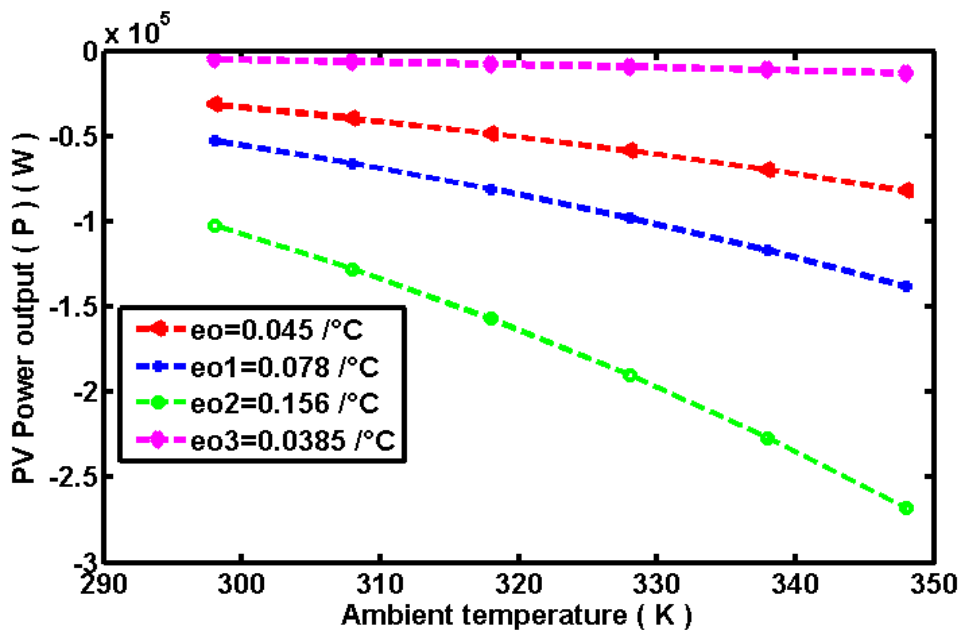
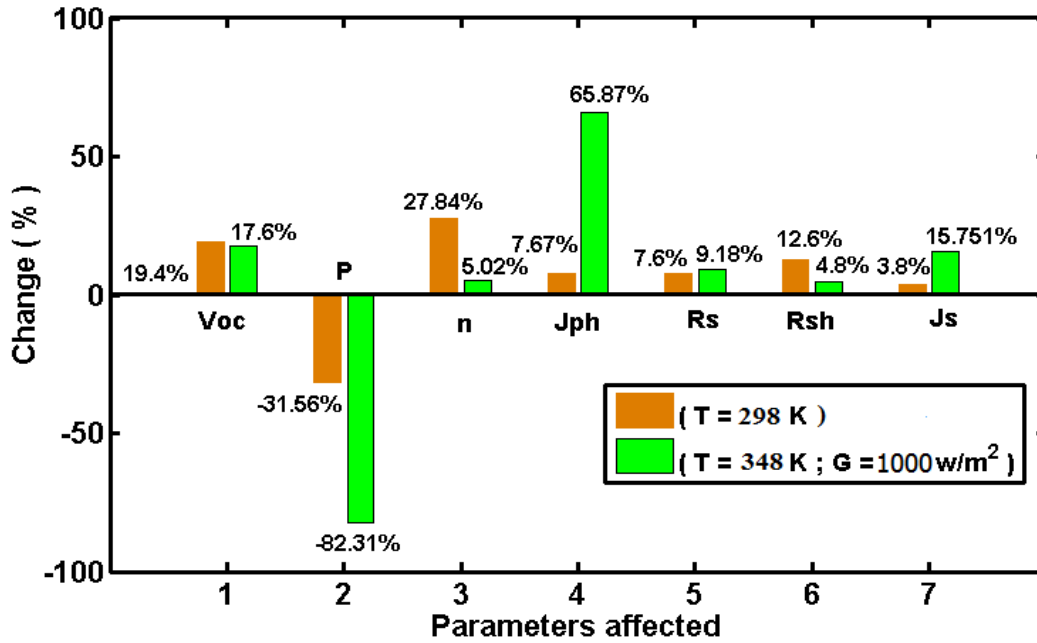


Fig.16. Variation of PV module output (P) with temperature in the range 295-348 K. This curve is analytically obtained from (Eq.46) as a function of the ambient temperature



**Fig.17. Overall Statistical Results**

Globally, we note a small increase in saturation current density ( $J_S$ ) by 3.8% and 15.76% with temperature, which can be attributed to the increased light absorption owing to a decrease in the bandgap of silicon. The decrease of ( $\eta$ ) with temperature is mainly controlled by the decrease of ( $V_{OC}$ ) and fill factor (FF) with T. It can be seen that with the temperature increasing, the ( $J_{SC}$ ) increases slightly and the ( $V_{OC}$ ) decreases strongly. The slight increase of ( $J_S$ ) in this study, similar to the effects of ( $J_{SC}$ ) originates from the narrowing of the band gap along with the increase in the number of phonons and density of states in the conduction and valence bands, while the strong decrease in the ( $V_{OC}$ ) is mainly linked to the increase of the leakage current [90]. For a standard solar cell, the ( $J_{SC}$ ) can be strongly influenced by the minority carrier diffusion length which depends on the product of the minority electron mobility and carrier lifetime. In addition, the rate of decrease of ( $V_{OC}$ ) is 7.8% and is much larger in magnitude than decrease of  $R_s$  with T. The rate of decrease in the maximum output power (P) is 50.75% while that of the efficiency ( $\eta$ ) is about 22.82%. This result is very significant in our work because, the effect of heat and irradiance are the factors that negatively affect the overall performance of PV cells.

Moreover, the impact of non-linearity of the ( $J_S$ ) (**Fig.17**) with irradiance or T in this study is very small for silicon solar cell.

#### 4. Conclusions and perspectives

Monocrystalline silicon PV cells/modules degradation has been investigated analytically in this work, under temperature and heat effect, using the Servant model under standard irradiation conditions ( $G=1000 \text{ W/m}^2$ ) in the 298-348K temperature range. Next, the single exponential model has been used to extract the PV cell parameters from a single ( $J$ - $V$ ) characteristic curve at various values of  $T$ . Finally, the different failure modes of PV cells/modules induced by heat and temperature have been indexed.

Our results reveal that:

- Delamination of encapsulant and back sheet,
- Bubble formation, Oxidation of busbars, Yellowing / browning of encapsulants and back sheets with and without power loss,
- Discoloration of busbars,
- Corrosion of connections,
- Cracking of back sheet,
- Hot spots, Cell breakage and micro cracks are the dominant modes of degradation,
- Temperature is responsible for most of the chemical reactions, and extremely significant to the PV modules degradation process; especially hot spots, encapsulant bleaching, and delamination failure on interconnections, corrosion, discoloration, and bubbles on the panel's surface.

The numerical simulated show that ( $J_{ph}$ ) increase exponentially from 7.67% to 65.87% with temperature. ( $R_s$ ) increase linearly by 7.6% and 9.18% while ( $V_{OC}$ ) decrease from 19.4 % to 17.6% and ( $R_{sh}$ ) decrease approximately by 12.6% and 4.8%. The power output ( $P$ ) losses decreases by 82.31 % and 31.56%, and the overall linear losses in efficiency ( $\eta$ ) has been approximately 27.84% and 5.02%, while ( $J_s$ ) increase exponentially from 3.87% to 15.75%.

In definitive, the increase in ( $J_{ph}$ ) with temperature can be attributed to the increased in light absorption owing to a decrease in the bandgap of silicon. The decrease in ( $\eta$ ) with temperature is mainly controlled by the decrease in ( $V_{OC}$ ) and fill factor (FF) with  $T$ . Elevated temperatures can drastically change the mechanical, electrical, and optical

properties of polymeric materials, as a result, a drop of the PV cells/modules overall efficiency.

Future work can be about:

- 1- Extensions to the model,
- 2- Improvement of the analytical results,
- 3- Compare experimental results obtained by Mattei model with those obtained analytically,
- 4- Compare analytically Servant model with Mattei model.

### **Acknowledgements**

I grateful to Professor Basile Bruno Kounouhéwa, Dr. Vianou Irénée Madogni and Dr. Macaire Agbomahéna for fruitful discussions. I acknowledge “Laboratoire de Physique du Rayonnement LPR, FAST-UAC 01BP 526 Cotonou, Benin”.

### **Competing Interests**

Authors have declared that no competing interests exist.

### **References**

1. Ababacar N, Abdérafi C, Abdessamad K, Cheikh M F K, Pape A N, Vincent S. Degradations of silicon photovoltaic modules: A literature review. *Solar Energy*. 2013; 96:140-151.
2. Vianou I M, Basile K, Idriss A Y, Macaire A, Etienne H, Clément K, Cossi N A. Modèle analytique pour l'étude de la dégradation de la performance des cellules photovoltaïques au silicium monocristallin. *Afrique SCIENCE*. 2016;12:182-200.
3. Munoz M A, Alonso-Garcia M C, Nieves V, Chenlo F. Early degradation of silicon PV modules and guaranty conditions. *Solar Energy*. 2011; 85:2264-2274.
4. Osterwald C R, McMahon T J. History of accelerated and qualification testing of terrestrial photovoltaic modules: a literature review. *Progress in Photovoltaics: Research and Applications*. 2009;17:11-33.
5. Vazquez M, Ignacio R S. Photovoltaic module reliability model based on field degradation studies. *Progress in Photovoltaics: Research and Applications*. 2008;16:419-433.
6. Kurtz S, Whitfield K, Tamizhmani G, Koehl M, Miller D, Joyce J, Wohlgemuth J, Bosco N, Kempe M, Zgonena T. Evaluation of high-temperature exposure of

photovoltaic modules. *Progress in Photovoltaics: Research and Applications*. 2011;12:954-965.

7. Swapnil D, atin Narotam S, Bharath S. Temperature Dependent Photovoltaic (PV) Efficiency and Its Effect on PV Production in the World A Review. *Energy Procedia*. 2013;33:311-321.

8. Alexander P, Nitsa K, George M, George E G. Review of photovoltaic degradation rate methodologies. *Renewable and Sustainable Energy Reviews*. 2014;40:143-152.

9. Reis A M, Coleman N T, Marshall M W, Lehman P A, Chamberlin C E. Comparison of PV module performance before and after 11-years of field exposure. 29<sup>th</sup> IEEE Photovoltaic Specialists Conference - PVSC, New Orleans. 2002;1432-1435.

10. Sánchez-Friera P, Piliougine M, Peláez J, Carretero J, Sidrach de Cardona M. Analysis of degradation mechanisms of crystalline silicon PV modules after 12 years of operation in Southern Europe. *Progress in photovoltaics: Research and Applications*. 2011;19:658-66.

11. Sakamoto S, Oshiro T. Field test results on the stability of crystalline silicon photovoltaic modules manufactured in the 1990s. In: *Proceedings of the 3<sup>rd</sup> world conference on photovoltaic energy conversion*. 2003;1888-1891.

12. Hishikawa Y, Morita K, Sakamoto S, Oshiro T. Field test results on the stability of 2400 photovoltaic modules manufactured in 1990s. *International Proceedings of the 29th IEEE photovoltaic specialists conference*. 2002;1687-1690.

13. Quintana M A, King D L, McMahon T J, Osterwald C R, Commonly observed degradation infield-aged photovoltaic modules. *International Proceedings of the 29<sup>th</sup> IEEE photovoltaic specialists conference*. 2002;1436-1439.

14. Fairouz I, Rabah M, Djamil A. Competing Risk of Degradation Processes of a Photovoltaic System under Several Conditions. *International Journal of Electrical Energy*. 2014;2:295-299.

15. Zimmerman C G. Time dependent degradation of photovoltaic modules by ultraviolet light. *Applied Physics Letter*. 2008;92:241110.

16. Skoczek A, Sample T, Dunlop E D, Ossenbrink, H A. Electrical performance results from physical stress testing of commercial PV modules to the IEC61215 test sequence. *Solar Energy Materials and Solar Cells*. 2008;92:1593-1604.

17. Oreski G, Wallner G M. Aging mechanisms of polymeric films for PV encapsulation. *Solar Energy*. 2005;79:612-617.

18. Jansen, K. W, Delahoy, A E. A laboratory technique for the evaluation of electrochemical transparent conductive oxide delamination from glass substrates. *Thin Solid Films*. 2003;423:153-160.
19. Kaplanis S, Kaplani E. Energy performance and degradation over 20 years performance of BP c-Si PV modules. *Simulation Modeling Practice and Theory*. 2011;19:1201-1211.
20. Wohlgemuth J H, Kurtz S. Reliability Testing Beyond Qualification as a Key Component in Photovoltaic's Progress Toward Grid Parity. In: *IEEE International Reliability Physics Symposium Monterey, California, 10-14 April; 2011*.
21. Oreski G, Wallner G M. Evaluation of the aging behavior of ethylene copolymer films for solar applications under accelerated weathering conditions. *Solar Energy*. 2009;83:1040-1047.
22. Berman D, Faiman D. EVA browning and the time-dependence of I-V curve parameters on PV modules with and without mirror- enhancement in a desert environment. *Solar Energy Materials and Solar Cells*. 2007;45:401-412.
23. Kempe M D. Ultraviolet test and evaluation methods for encapsulants of photovoltaic modules. *Solar Energy Materials and Solar Cells*. 2010;94:246-253.
24. Rueland E, Herguth A, Trummer A, Wansleben S, Fath P. Optical l-crack detection in combination with stability testing for inline inspection of wafers and cells. In: *Proceedings of 20th EU PVSEC, Barcelona*. 2005;3242-3245.
25. Molenbroek E, Waddington D W, Emery K A. Hot spot susceptibility and testing of PV modules, *International Conference Record of the 22th IEEE*. 1991;1:547-552.
26. Herrmann W, Wiesner W, Vaassen W. Hot spot investigations on PV modules- new concepts for a test standard and consequences for module design with respect to bypass diodes, *International Conference Record of the 26th IEEE, Anaheim*. 1997;1129-1132.
27. Stephan M, Thomas K, Wolfgang J, Hurbert F. Quality testing for PV modules according to standards and performance control for supporting manufacturing. In: *Proceedings of the 19th EU PVSEC, Paris; 2004*.
28. Iwahashi T, Morishima M, Fujibayashi T, Yang R, Lin J, Matsunaga D. Silicon nitride anti-reflection coating on the glass and transparent conductive oxide interface for thin film solar cells and modules. *Journal of applied physics*. 2015;118:145302.

29. McIntosh K R, Powell N E, Norris A W, Cotsell J N, Ketola B M. The effect of damp heat and UV aging tests on the optical properties of silicone and EVA encapsulants. *Progress in Photovoltaic Research and Application*. 2011;19:294-300.
30. Staebler D L, Wronski C R. Reversible conductivity changes in discharge-produced amorphous Si. *Applied Physics Letters*. 1977;31:292.
31. Biswas R, Kwon I, Soukoulis C M. Mechanism for the Staebler Wronski effect in a-Si:H. *Physical Review B*. 1991;44:3403-3406.
32. Polverini D, Field M, Dunlop E, Zaaiman W; Polycrystalline silicon PV modules performance and degradation over 20 years. *Progress in Photovoltaics: Research and Applications*; 2013;21:1004-1015.
33. Park S, Dhakal R, Lehman L, Cotts E. Measurement of deformations in SnAgCu solder interconnects under in situ thermal loading. *Acta Materialia*. 2007;55:3253-3260.
34. McMahon T J. Accelerated testing and failure of thin-film PV modules. *Progress in Photovoltaics: Research and Applications*. 2004;12:235-248.
35. Kempe M D. Modeling of rates of moisture ingress into photovoltaic modules. *Solar Energy Material Solar Cells*. 2006;90:2720-2738.
36. Siddiqui M U, Abido M. Parameter estimation for five and seven-parameter photovoltaic electrical models using evolutionary algorithms. *Applied Soft Computing*. 2013;13:4608-4621.
37. Ma T, Yang H, Lu L. Development of a model to simulate the performance characteristics of crystalline silicon photovoltaic modules/strings/arrays. *Solar Energy*. 2014;100:31-41.
38. Bai J, Liu S, Hao Y, Zhang Z, Jiang M, Zhang Y. Development of a new compound method to extract the five parameters of PV modules. *Energy Conversion and Management*. 2014;79:294-303.
39. Attivissimo F, Adamo F, Carullo A, Lanzolla A M L, Spertino, F, Vallan, A. On the performance of the double-diode model in estimating the maximum power point for different photovoltaic technologies. *Measurement*. 2013;46:3549-3559.
40. Ishaque K, Salam Z, Syafaruddin A. Comprehensive MATLAB Simulink PV system simulator with partial shading capability based on two-diode model. *Solar Energy*. 2011;85:2217-2227.
41. Ishaque K, Salam Z, Taheri H. Simple, fast and accurate two-diode model for photovoltaic modules. *Solar Energy Materials and Solar Cells*. 2011;95:586-594.

42. Tossa A K, Soro Y M, Azoumah Y, Yamegueu D. A new approach to estimate the performance and energy productivity of photovoltaic modules in real operating conditions. *Solar Energy*. 2014;110:543-560.
43. Ghani F, Duke M, Carson J. Numerical calculation of series and shunt resistance of a photovoltaic cell using the Lambert W-function: experimental evaluation. *Solar Energy*. 2013;87:246-253.
44. Ghani F, Duke M. Numerical determination of parasitic resistances of a solar cell using the Lambert W-function. *Solar Energy*. 2011;85:2386-2394.
45. Luque A, Hegedus S. *Handbook of Photovoltaic Science and Engineering*. Wiley, Hoboken, N J; 2003.
46. Gow J A, Manning C D. Development of a photovoltaic array model for use in power electronics simulation studies. In: *IEEE Proceedings of Electric Power Applications*. 1999;146:193-200.
47. Lun S, Du C, Guo T, Wang S, Sang J, Li J. A new explicit IV model of a solar cell based on Taylor's series expansion. *Solar Energy*. 2013;94:221-232.
48. Kulaksiz A A, ANFIS-based estimation of PV module equivalent parameters: application to a stand-alone PV system with MPPT controller Turk. *Journal of Electronic Engineering and Computer Science*. 2013;21:2127-2140.
49. Kaminski A, Marchand J J, Laugier, A. Methods to extract junction parameters with special emphasis on low series resistance. *Solid State Electronic*. 1999;43:741-745.
50. De Soto W, Klein S.A, Beckman W A. Improvement and validation of a model for photovoltaic array performance. *Solar Energy*. 2006;80:78-88.
51. Yordanov G H, Midtgard O M. Physically consistent parameterization in the modeling of solar photovoltaic devices, In: *Power Tech, IEEE Trondheim*. 2011;1-4.
52. Arora J D, Verma A V, Bhatnagar, M. Variation of series resistance with temperature and illumination level in diffused junction poly- and single-crystalline silicon solar cells. *Journal Materials Science Letters*. 1986;5:1210-1212.
53. Jinlei Ding, Xiaofang Cheng, Tairan Fu. Analysis of series resistance and P-T characteristics of the solar cell. *Vacuum*. 2005;77:163-167.
54. Deshmukh M P, Nagaraju J. Measurement of silicon and GaAs/Ge solar cell device parameters. *Solar Energy Materials and Solar Cells*. 2005;89:403-408.

55. Radziemska E, Klugmann E. Thermally affected parameters of the current-voltage characteristics of silicon photocell. *Energy Conversion and Management*. 2002;43:1889-1900.
56. Chakrabarty K, Singh S N. Depletion layer resistance and its effect on I-V characteristics of fully and partially-illuminated silicon solar cells. *Solid State Electronics*. 1996;39:577.
57. Alonso Garcia M C, Balenzategui, J L. Estimation of photovoltaic module yearly temperature and performance based on Nominal Operation Cell Temperature calculations. *Renewable Energy*. 2004;29:1997-2010.
58. Skoplaki E, Palyvos, J A. On the temperature dependence of photovoltaic module electrical performance: A review of efficiency/power correlations. *Solar Energy*. 2009;83:614-624
59. Zondag H A. Flat-plate PV-thermal collectors and systems - a review. *Renewable and Sustainable Energy Reviews*. 2008;12:891-959.
60. Garg H P, Agarwal R K. Some aspects of a PV/T collector/forced circulation flat plate solar water heater with solar cells. *Energy Conversion and Management*. 1995;36:87-99.
61. Evans D L, Florschuetz L W. Terrestrial concentrating photovoltaic power system studies. *Solar Energy*. 1978;20:37-43.
62. Evans, D L. Simplified method for predicting photovoltaic array output. *Solar Energy*. 1981;27:555-560.
63. Kou Q, Klein S A, Beckman W A. A method for estimating the long-term performance of direct-coupled PV pumping systems. *Solar Energy*. 1998;64:33-40.
64. Siegel M D, Klein S A, Beckman W A. A simplified method for estimating the monthly-average performance of photovoltaic systems. *Solar Energy*. 1981;26:413-418.
65. Jie J, Hua Y, Gang P, Bin J, Wei H. Study of PV-Trombe wall assisted with DC fan. *Building and Environment*. 2007;42:3529-3539.
66. Rosell J I, Ibanez M. Modeling power output in photovoltaic modules for outdoor operating conditions. *Energy Conversion and Management*. 2006;47:2424-2430.
67. Furushima K, Nawata Y, Sadatomi M. Prediction of photovoltaic power output considering whether effects. In: *ASES Conference Solar Renewable Energy Key to Climate Recovery July 7–13, Denver, Colorado; 2006*.

68. Farmer B K. PVUSA Model Technical Specification for a Turnkey Photovoltaic Power System;1992.
69. Meyer E L, Van Dyk E E, Development of energy model based on total daily irradiation and maximum ambient temperature. *Renewable Energy*. 2000;21:37-47.
70. Taylor R W. System and module rating: advertised versus actual capability. *Solar Cells*. 1986;18:335-344.
71. Jie J, Wei H, Lam H N. The annual analysis of the power output and heat gain of a PV-wall with different integration mode in Hong Kong. *Solar Energy Materials and Solar Cells*. 2002;71:435-448.
72. Mattei M, Notton G, Cristofari C, Muselli M, Poggi P. Calculation of the polycrystalline PV module temperature using a simple method of energy balance. *Renewable Energy*. 2006;31:553-567.
73. Koehl M, Heck M, Wiesmeier S, Wirth J. Modeling of the nominal operating cell temperature based on outdoor weathering. *Solar Energy Materials and Solar Cells*. 2011;95:1638-1646.
74. Patricia M S, Jesus C, Mariano S C, Models to predict the operating temperature of different photovoltaic modules in outdoor conditions. *Progress in Photovoltaics: Research and Applications*. 2015;23:1267-1282.
75. Boddaert S, Chervet F. Long-term experimental validation of NOCT method for PV integration under several conditions. *Proceedings of 27<sup>th</sup> European Photovoltaic Solar Energy Conference*. 2012;3946-3950.
76. Servant J, Calculation of cell temperature for photovoltaic modules from climatic data, *Proceedings of the 9th Biennial Congress of the International Solar Energy Society- Intersol, Montreal, Canada*. 1976; 3:1640-1643.
77. Ross R G, Interface design considerations for terrestrial solar cell modules, *Proceedings of the 12<sup>th</sup> IEEE photovoltaic Specialists conference, Baton Rouge, L A, November*. 1976;15-18:801-806.
78. King D, Boyson W, Kratochvil J. Photovoltaic array performance model. Sandia National Laboratories. Report SAND2004-3535. Available from: <http://prod.sandia.gov/techlib/access-control.cgi/2004/043535.pdf> accessed 3 January; 2014.
79. Evdokimov V M, Maiorov V A. A Study of Limiting Energy and Temperature Characteristics of Photovoltaic Solar Radiation Converters. *Applied Solar Energy*. 2017;1-9.

- 80.** Shockley W, Queisser H J. Detailed Balance Limit of Efficiency of p-n Junction Solar Cells. *Journal of Applied Physics*. 1961;32:510-519.
- 81.** Deibel C, Dyakonov V. Polymer-Fullerene Bulk Heterojunction Solar Cells. *Reports on Progress in Physics*. 2010;73:096401.
- 82.** Nyman M. Interfacial Effects in Organic Solar Cells, PhD dissertation, Abo Akademi University, Finland; 2015.
- 83.** Kazem H A, Khatib T, Sopian K , Buttinger F, Elmenreich W, Albusaidi A S. Effect of Dust Deposition on the Performance of Multi-Crystalline Photovoltaic Modules Based on Experimental Measurements. *International Journal of Renewable Energy Research*. 2013;3:850-853.
- 84.** Manganiello P, Balato M, Vitelli M. A survey on mismatching and aging of PV modules: the closed loop. *IEEE Trans Ind Electron*. 2015; 6: 7276-86.
- 85.** Tamizhmani G, Kuitche J. Accelerated lifetime testing of photovoltaic modules. Solar America Board for Codes and Standards. Photovoltaic Reliability Laboratory. Arizona State University; 2013.
- 86.** Park N C, Joeng J S, Kang B J, Kim D H. The effect of encapsulant discoloration and delamination on the electrical characteristics of photovoltaic module. *Microelectronic Reliability*. 2013;53:1818-22.
- 87.** Pramod R, Tiwari G N, Sastry O S, Birinchi B, Vikrant S, Degradation of monocrystalline photovoltaic modules after 22 years of outdoor exposure in the composite climate of India. *Solar Energy*. 2016; 135: 786-795.
- 88.** Oreski G, Pinter G. Comparative study of the temperature dependent delamination behavior of four solar cell encapsulants to glass and backsheet-laminate. In: 26<sup>th</sup> European Photovoltaic Solar Energy Conference and Exhibition. 2011; 3305-3309.
- 89.** Claudio F, Daniel P. Why Do PV Modules Fail. *Energy Procedia*. 2012;15:379 -387.
- 90.** Chengquan X, Xuegong Y, Deren Y, Duanlin Q. Impact of solar irradiance intensity and temperature on the performance of compensated crystalline silicon solar cells. *Solar Energy Materials & Solar Cells*. 2014; 128: 427-434.